High organic inputs explain shallow and deep SOC storage in a long-term agroforestry system – Combining experimental and modeling approaches.

Rémi Cardinael[a,b,c*], Bertrand Guenet[d], Tiphaine Chevallier[a], Christian Dupraz[e], Thomas Cozzi[b], Claire Chenu[b]

[a] IRD, UMR Eco&Sols, Montpellier SupAgro, 2 place Viala, 34060 Montpellier, France

[b] AgroParisTech, UMR Ecosys, Avenue Lucien Brétignières, 78850 Thiverval-Grignon, France

[c] CIRAD, UPR AIDA, Avenue d'Agropolis, 34398 Montpellier, France (present address)

[d] Laboratoire des Sciences du Climat et de l'Environnement, UMR CEA-CNRS-UVSQ, CE L'Orme des Merisiers, 91191 Gif-Sur-Yvette, France

[e] INRA, UMR System, Montpellier SupAgro, 2 place Viala, 34060 Montpellier, France

* Corresponding author. Tel.: +33 04.67.61.53.08. E-mail address: remi.cardinael@cirad.fr

Keywords: priming effect, deep roots, deep soil organic carbon, spatial heterogeneity, silvoarable system, crop yield, SOC modeling

Abstract

Agroforestry is an increasingly popular farming system enabling agricultural diversification and providing several ecosystem services. In agroforestry systems, soil organic carbon (SOC) stocks are generally increased, but it is difficult to disentangle the different factors responsible for this storage. Organic carbon (OC) inputs to the soil may be larger, but SOC decomposition rates may be modified owing to microclimate, physical protection, or priming effect from roots, especially at depth. We used an 18-year-old silvoarable system associating hybrid walnut trees (*Juglans regia* × *nigra*) and durum wheat (*Triticum turgidum* L. subsp. *durum*), and an adjacent

agricultural control plot to quantify all OC inputs to the soil - leaf litter, tree fine root senescence, crop residues, and tree row herbaceous vegetation -, and measure SOC stocks down 2 m depth at varying distances from the trees. We then proposed a model that simulates SOC dynamics in agroforestry accounting for both the whole soil profile and the lateral spatial heterogeneity. The model was calibrated to the control plot only.

Measured OC inputs to soil were increased by about 40% (+ 1.11 t C ha^{-1} yr^{-1}) down to 2 m depth in the agroforestry plot compared to the control, resulting in an additional SOC stock of 6.3 t C ha^{-1} down to 1 m depth. The model was strongly validated, describing properly the measured SOC stocks and distribution with depth in agroforestry tree rows and alleys. It showed that the increased inputs of fresh biomass to soil explained the observed additional SOC storage in the agroforestry plot. Moreover, only a priming effect variant of the model was able to capture the depth distribution of SOC stocks. Modeling revealed a strong priming effect that would reduce the potential SOC storage due to higher organic inputs in the agroforestry system by 75 to 90%. This result questions the potential of soils to store large amounts of carbon, especially at depth. Deep-rooted trees modify OC inputs to soil, a process that deserves further studies given its potential effects on SOC dynamics.

1 Introduction

Agroforestry systems are complex agroecosystems combining trees and crops or pastures within the same field (Nair, 1993, 1985; Somarriba, 1992). More precisely, silvoarable systems associate parallel tree rows with annual crops. Some studies showed that these systems could be very productive, with a land equivalent ratio (Mead and Willey, 1980) reaching up to 1.3 (Graves et al., 2007). Silvoarable systems may therefore produce up to 30% more marketable biomass on the same area of land compared to crops and trees grown separately. This performance can be explained by a better use of water, nutrients and light by the agroecosystem

51 throughout the year. Trees grown in silvoarable systems usually grow faster than the same trees
52 grown in forest ecosystems, because of their lower density, and because they also benefit from
53 the crop fertilization (Balandier and Dupraz, 1999; Chaudhry et al., 2003; Chifflot et al., 2006).
54 In temperate regions, farmers usually grow one crop per year, and this association of trees can
55 extend the growing period at the field scale, especially when winter crops are intercropped with
56 trees having a late bud break (Burgess et al., 2004). However, after several years, a decrease of
57 crop yield can be observed in mature and highly dense plantations, especially close to the trees,
58 due to competition between crops and trees for light, water, and nutrients (Burgess et al., 2004;
59 Dufour et al., 2013; Yin and He, 1997).
60 Part of the additional biomass produced in agroforestry is used for economical purposes, such
61 as timber or fruit production. Leaves, tree fine roots, pruning residues and the herbaceous
62 vegetation growing in the tree rows will usually return to the soil, contributing to a higher input
63 of organic carbon (OC) to the soil compared to an agricultural field (Peichl et al., 2006).
64 In such systems, the observed soil organic carbon (SOC) stocks are also generally higher
65 compared to a cropland (Albrecht and Kandji, 2003; Kim et al., 2016; Lorenz and Lal, 2014).
66 Cardinael *et al.*, (2017) measured a mean SOC stock accumulation rate of 0.24 (0.09-0.46) t C
67 ha^{-1} yr^{-1} at 0-30 cm depth in several silvoarable systems compared to agricultural plots in
68 France. Higher SOC stocks were also found in Canadian agroforestry systems, but measured
69 only to 20 cm depth (Bambrick et al., 2010; Oelbermann et al., 2004; Peichl et al., 2006).
70 To our knowledge, we are still not able to disentangle the factors responsible for such a higher
71 SOC storage. This SOC storage might be due to higher OC inputs but it could also be favored
72 by a modification of the SOC decomposition owing to a change in SOC physical protection
73 (Haile et al., 2010), and/or in soil temperature and moisture.
74 The introduction of trees in an agricultural field modifies the amount, but also the distribution
75 of fresh organic carbon (FOC) input to the soil, both vertically and horizontally (Bambrick et

al., 2010; Howlett et al., 2011; Peichl et al., 2006). FOC inputs from the trees decrease with increasing distance from the trunk and with soil depth (Moreno et al., 2005). On the contrary, crop yield usually increases with increasing distance from the trees (Dufour et al., 2013; Li et al., 2008). Therefore, the proportions of FOC coming from both the crop residues and the trees change with distance from the trees, soil depth, and time.

Tree fine roots (diameter ≤ 2 mm) are the most active part of root systems (Eissenstat and Yanai, 1997) and play a major role in carbon cycling. In silvoarable systems, tree fine root distribution within the soil profile is strongly modified due to the competition with the crop, inducing a deeper rooting compared to trees grown in forest ecosystems (Cardinael et al., 2015a; Mulia and Dupraz, 2006). Deep soil layers may therefore receive significant OC inputs from fine root mortality and exudates. Root carbon has a higher mean residence time in the soil compared to shoot carbon (Kätterer et al., 2011; Rasse et al., 2006), presumably because root residues are preferentially stabilized within microaggregates or adsorbed to clay particles. Moreover, temperature and moisture conditions are more buffered in the subsoil than in the topsoil. The microbial biomass is also smaller at depth (Eilers et al., 2012; Fierer et al., 2003), and the spatial segregation with organic matter is larger (Salomé et al., 2010) resulting in lower decomposition rates. Deep root carbon input in the soil could therefore contribute to a SOC storage with high mean residence times. However, some studies showed that adding FOC – a source of energy for microorganisms - to the subsoil enhanced decomposition of stabilized carbon, a process called « priming effect » (Fontaine et al., 2007). The priming effect is stronger when induced by labile molecules like root exudates than by root litter coming from the decomposition of dead roots (Shahzad et al., 2015). Therefore, the net effect of deep roots on SOC stocks has to be assessed, especially in silvoarable systems.

Models are crucial as they allow virtual experiments to best design and understand complex processes in these systems (Luedeling et al., 2016). Several models have been developed to

simulate interactions for light, water and nutrients between trees and crops (Charbonnier et al., 2013; Duursma and Medlyn, 2012; van Noordwijk and Lusiana, 1999; Talbot, 2011) or to predict tree growth and crop yield in agroforestry systems (Graves et al., 2010; van der Werf et al., 2007). However, none of these models are designed to simulate SOC dynamics in agroforestry systems and they are therefore not useful to estimate SOC storage. Oelbermann & Voroney (2011) evaluated the ability of the CENTURY model (Parton et al., 1987) to predict SOC stocks in tropical and temperate agroforestry systems, but with a single-layer modeling approach (0-20 cm). The approach of modeling a single topsoil layer assumes that deep SOC does not play an active role in carbon cycling, while it was shown that deep soil layers contain important amounts of SOC (Jobbagy and Jackson, 2000), and that part of this deep SOC could cycle on decadal timescales due to root inputs or to dissolved organic carbon transport (Baisden and Parfitt, 2007; Koarashi et al., 2012). The need to take into account deep soil layers when modeling SOC dynamics is now well recognized in the scientific community (Baisden et al., 2002; Elzein and Balesdent, 1995), and several models have been proposed (Braakhekke et al., 2011; Guenet et al., 2013; Koven et al., 2013; Taghizadeh-Toosi et al., 2014; Ahrens et al., 2015). Using vertically discretized soils is particularly important when modeling the impact of agroforestry systems on SOC stocks, but to our knowledge, vertically spatialized SOC models have not yet been tested for these systems.

The aims of this study were then twofold: (i) to propose a model of soil C dynamics in agroforestry systems able to account for both vertical and lateral spatial heterogeneities and (ii) to test whether variations of fresh organic carbon (FOC) input could explain increased SOC stocks both using experimental data and model runs.

For this, we first compiled data on FOC inputs to the soil obtained in a 18-year-old agroforestry plot and in an agricultural control plot in southern France, in which SOC stocks have been

recently quantified to 2 m depth (Cardinael et al., 2015b). FOC inputs comprised tree fine roots, tree leaf litter, aboveground and belowground biomass of the crop and of the herbaceous vegetation in the tree rows. We compiled recently published data for FOC inputs (Cardinael et al., 2015a; Germon et al., 2016), and measured the others (Table 1).

We then modified a two pools model proposed by Guenet *et al.*, (2013), to create a spatialized model over depth and distance from the tree, the CARBOSAF model (soil organic CARBOn dynamics in Silvoarable AgroForestry systems). Based on data acquired since the tree planting in 1995 (crop yield, tree growth), and on FOC inputs, we modeled SOC dynamics to 2 m depth in both the silvoarable and agricultural control plot. We evaluated the model against measured SOC stocks along the profile and used this opportunity to test the importance of priming effect (*PE*) for deep soil C dynamics in a silvoarable system. The performance of the two pools model including *PE* was also compared with a model version including three OC pools.

2 Materials and methods

2.1 Study site

The experimental site is located at the Restinclières farm Estate in Prades-le-Lez, 15 km North of Montpellier, France (longitude 04°01' E, latitude 43°43' N, elevation 54 m a.s.l.). The climate is sub-humid Mediterranean with an average temperature of 15.4°C and an average annual rainfall of 973 mm (years 1995–2013). The soil is a silty and carbonated (pH = 8.2) deep alluvial Fluvisol (IUSS Working Group WRB, 2007). In February 1995, a 4.6 hectare silvoarable agroforestry plot was established with the planting of hybrid walnut trees (*Juglans regia* × *nigra* cv. NG23) at a density of 192 trees ha^{-1} but later thinned to 110 trees ha^{-1}. Trees were planted at 13 m × 4 m spacing, and tree rows are East–West oriented. The cultivated alleys are 11 m wide. The remaining part of the plot (1.4 ha) was kept as an agricultural control plot.

Since the tree planting, the agroforestry alleys and the control plot were managed in the same way. The associated crop is most of the time durum wheat (*Triticum turgidum* L. subsp. *durum*), except in 1998, 2001 and 2006, when rapeseed (*Brassica napus* L.) was cultivated, and in 2010 and 2013, when pea (*Pisum sativum* L.) was cultivated. The soil is ploughed to a depth of 0.2 m before sowing, and the wheat crop is fertilized with an average of 120 kg N ha^{-1} yr^{-1}. Crop residues (wheat straw) are also exported, but about 25% remain on the soil. Tree rows are covered by spontaneous herbaceous vegetation. Two successive herbaceous vegetation types occur during the year, one in summer and one in winter. The summer vegetation is mainly composed of *Avena fatua* L., and is 1.5 m tall. In winter, the vegetation is a mix of *Achillea millefolium* L., *Galium aparine* L., *Vicia* L., *Ornithogalum umbellatum* L. and *Avena fatua* L, and is 0.2 m tall.

Table 1. Synthesis of the different field and laboratory data available or measured, and their sources.

Description of the data	Source
Soil texture, bulk densities, SOC stocks	Cardinael *et al.*, (2015a)
Soil temperature and soil moisture	Measured
Tree growth (DBH)	Measured
Tree wood density	(Talbot, 2011)
Tree fine root biomass	Cardinael *et al.*, (2015b)
Tree fine root turnover	Germon *et al.*, (2016)
Crop yield and crop ABG biomass	Dufour *et al.*, (2013) and measured
Crop root biomass	Prieto *et al.*, (2015) and measured
Tree row herbaceous vegetation – ABG biomass	Measured
Tree row herbaceous vegetation – root biomass	Measured
Biomass carbon concentrations	Measured
Potential decomposition rate of roots	Prieto *et al.*, (2016a)
HSOC potential decomposition rate	Measured

DBH: Diameter at Breast Height; ABG: aboveground; OC: organic carbon; HSOC: humified soil organic carbon.

2.2 Organic carbon stocks

2.2.1 Soil organic carbon stocks

SOC data have been published in Cardinael *et al.*, (2015b). Briefly, soil cores were sampled down to 2 m depth in May 2013, 100 in the agroforestry plot, and 93 in the agricultural control plot. SOC concentrations, soil bulk densities, SOC stocks, and soil texture were measured for ten soil layers (0.0-0.1, 0.1-0.3, 0.3-0.5, 0.5-0.7, 0.7-1.0, 1.0-1.2, 1.2-1.4, 1.4-1.6, 1.6-1.8, and 1.8-2.0 m). In the agroforestry plot, 40 soil cores were taken in the tree rows, while 60 were sampled in the alleys at varying distances from the trees. Soil organic carbon stocks were quantified on an equivalent soil mass basis (Ellert and Bettany, 1995).

2.2.2 Tree aboveground and stump carbon stocks

Three hybrid walnuts were chopped down in 2012. The trunk circumference was measured every meter up to the maximum height of the tree to estimate its volume. The trunk biomass was estimated by multiplying the trunk volume by the wood density that was measured at 616 kg m^{-3} during a previous work at the same site (Talbot, 2011). Then, branches were cut, the stump was uprooted, and they were weighted separately. Samples were brought to the laboratory to determine the moisture content, which enabled calculation of the branches and the stump dry mass.

2.3 Measurements of organic carbon inputs in the field

2.3.1 Carbon inputs from tree fine root mortality

The tree fine root (diameter $\leq$ 2 mm) biomass was quantified and coupled with an estimate of the tree fine root turnover in order to predict the carbon input to the soil from the tree fine root mortality. A detailed description of the methods used to estimate the tree fine root biomass can be found in Cardinael *et al.*, (2015a). In March 2012, a 5 (length) × 1.5 (width) × 4 m (depth) pit was open in the agroforestry plot, perpendicular to the tree row, at the North of the trees.

194 The tree fine root distribution was mapped down 4 m depth, and the tree fine root biomass was
195 quantified in the tree row and in the alley. Only results concerning the first two meters of soil,
196 among those obtained by Cardinael *et al.*, (2015a) will be used here.
197 In July 2012, sixteen minirhizotrons were installed in the agroforestry pit, at 0, 1, 2.5 and 4 m
198 depth, and at two and five meters from the trees. The tree root growth and mortality was
199 monitored during one year using a scanner (CI-600 Root Growth Monitoring System, CID,
200 USA), and analyzed using the WinRHIZO Tron software (Régent, Canada). A detailed
201 description of the methods and of results used to estimate the tree fine root turnover can be
202 found in Germon *et al.*, (2016).
203
204 **2.3.2 Tree litterfall**
205 In 2009, the crowns of two walnut trees were packed with a net in order to collect the leaf
206 biomass from September to January. The same was done in 2012 with three other walnut trees.
207 The leaf litter was then dried, weighted and analyzed for C to quantify the leaf carbon input per
208 tree.
209
210 **2.3.3 Aboveground and belowground input from the crop**
211 Since the tree planting in 1995, the crop yield was measured 14 times (in 1995, 2000, 2002,
212 2003, 2004, 2005, 2007, 2008, 2009, 2010, 2011, 2012, 2013, and 2014), while the wheat straw
213 biomass and the total aboveground biomass were measured six times (in 2007, 2008, 2009,
214 2011, 2012, and 2014) in both the control and the agroforestry plot (Dufour et al., 2013), using
215 sampling subplots of 1 m^2 each. In the control plot, five subplots have been sampled while in
216 the agroforestry plot five transects have been sampled. Each transect was made of three
217 subplots, 2 m North from the tree, 2 m South from the tree, and 6.5 m from the tree (middle of
218 the alley). In March 2012, a 2 m deep pit was opened in the agricultural control plot (Prieto et

al., 2015), and the root biomass was quantified to the maximum rooting depth (1.5 m). The root:shoot ratio of durum wheat was measured in the control plot. We assumed that the crop root biomass turns out once a year, after the crop harvest.

2.3.4 Above and belowground input from the tree row herbaceous vegetation

As two types of herbaceous vegetation grow in the tree rows during the year, samples were taken in summer and winter. In late June 2014, twelve subplots of 1 m^2 each were positioned in the tree rows, around 4 walnut trees. In January 2015, six subplots of 1 m^2 each were positioned in the tree rows, around 2 walnut trees. The middle of each subplot was located at 1 m, 2 m and 3 m, respectively, from the selected walnut tree. All the aboveground vegetation was collected in each square. In the middle of each subplot, root biomass was sampled with a cylindrical soil corer (inner diameter of 8 cm). Soil was taken at three soil layers, 0.0-0.1, 0.1-0.3 and 0.3-0.5 m. In the laboratory, soil was gently washed with water through a 2 mm mesh sieve, and roots were collected. Roots from the herbaceous vegetation were easily separated manually from walnut roots, as they were soft and yellow compared to walnuts roots that were black. After being sorted out from the soil and cleaned, the root biomass was dried at 40°C and measured.

2.4 Carbon concentration measurements

All organic carbon measurements were performed with a CHN elemental analyzer (Carlo Erba NA 2000, Milan, Italy), after samples were oven-dried at 40°C for 48 hours (Table 2). Dry biomasses (t DM ha^{-1}) of each organic matter inputs were multiplied by their respective organic carbon concentrations (mg C g^{-1}) to calculate organic carbon stocks (t C ha^{-1}).

Table 2. Organic carbon concentrations and C:N ratio of the different types of biomass.

Type of biomass	Organic C concentration (mg C g^{-1})	C:N	Number of replicates
Walnut trunk	445.7 ± 1.0	159.1 ± 25.2	3
Walnut branches	428.6 ± 1.7	62.2 ± 11.7	3
Wheat straw	433.2 ± 0.7	55.5 ± 2.1	5
Wheat root	351.4 ± 19	24.8 ± 2.1	8
Walnut leaf	449.4 ± 3.7	49.1 ± 0.4	3
Walnut fine root	437.0 ± 3.3	28.6 ± 3.4	8
Summer vegetation (ABG)	448.4 ± 1.9	37.8 ± 2.2	5
Summer vegetation (roots)	314.5 ± 8.3	33.8 ± 1.7	6
Winter vegetation (ABG)	447.7 ± 5.3	11.2 ± 0.4	3
Winter vegetation (roots)	397.4 ± 5.0	24.7 ± 0.7	3

The organic matter called "vegetation" stands for the herbaceous vegetation that grows in the tree row. ABG: aboveground. Errors represent standard errors.

2.5 General description of the CARBOSAF model

2.5.1 Organic carbon decomposition

We adapted a model developed by Guenet et al. (2013) where total SOC is split in two pools, the FOC and the humified soil organic carbon (HSOC) for each soil layer (Fig. 1a). Input to the FOC pool comes from the plant litter and the distribution of this input within the profile is assumed to depend upon depth from the surface (z), distance from the tree (d), and time (t). Equations describing inputs to the FOC pool ($I_{t,z,d}$) at a given time, depth, and distance are fully explained in the Results.

The FOC mineralisation is assumed to be governed by first order kinetics, being proportional to the FOC pool, as given by:

$$\frac{\partial FOC_{t,z,d}}{\partial t} = -k_{FOC} \times FOC_{t,z,d} \times f_{clay,z} \times f_{moist,z} \times f_{temp,z} \qquad (1)$$

where $FOC_{t,z,d}$ is the FOC carbon pool (kg C m^{-2}) at a given time (t, in years), depth (z, in m) and distance (d, in m), and k_{FOC} is its decomposition rate. The potential decomposition rates of the different plant materials were assessed with a 16-week incubation experiment during a companion study at the site (Prieto et al., 2016). The decomposition rate k_{FOC} was weighted by

the respective contribution of each type of plant litter as a function of the tree age, soil depth and distance from the tree. The rate modifiers $f_{clay,z}$, $f_{moist,z}$ and $f_{temp,z}$ are functions depending respectively on the clay content, soil moisture and soil temperature at a given depth z, and range between 0 and 1.

The f_{clay} function originated from the CENTURY model (Parton et al., 1987):

$$f_{clay,z} = 1 - 0.75 \times Clay_z \qquad (2)$$

where $Clay_z$ is the clay fraction (ranging between 0 and 1) of the soil at a given depth z.

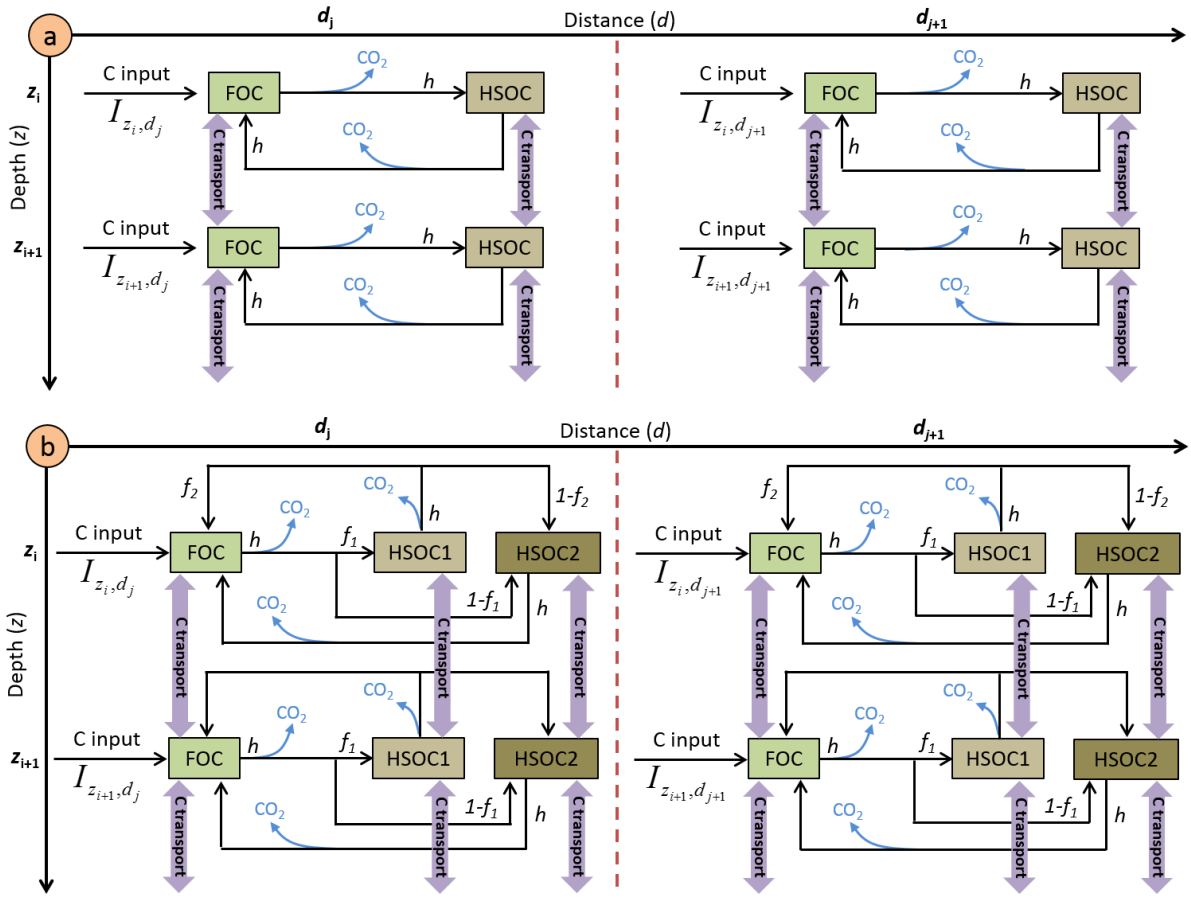

Fig. 1. Schematic representation of the pools and the fluxes of the (a) two pools model and (b) three pools model.

The $f_{moist,z}$ function originated from the meta-analysis of Moyano *et al.*, (2012) and is affected by soil properties (clay content, SOC content). Briefly, the authors fitted linear models on 310 soil incubations to describe the effect of soil moisture on decomposition. Then, they normalized such linear models between 0 and 1 to apply these functions to classical first order kinetics. All details are described in Moyano *et al.*, (2012). To save computing time, we calculated $f_{moist,z}$ only once using measured SOC stocks instead of using modelled SOC stocks and repeated the calculation at each time step.

The temperature sensitivity of the soil respiration is expressed as Q_{10}:

$$f_{temp,z} = Q_{10}^{\frac{temp_z - temp_{opt}}{10}} \quad (3)$$

with $temp_z$ being the soil temperature in K at each soil depth z and $temp_{opt}$ a parameter fixed to 304.15 K. The Q_{10} value was fixed to 2, a classical value used in models (Davidson and Janssens, 2006).

Once the FOC is decomposed, a fraction is humified (h) and another is respired as CO_2 ($1-h$) (Fig. 1a) following equations (4) and (5).

$$Humified\ FOC_{t,z,d} = h \times \frac{\partial FOC_{t,z,d}}{\partial t} \quad (4)$$

$$Respired\ FOC_{t,z,d} = (1-h) \times \frac{\partial FOC_{t,z,d}}{\partial t} \quad (5)$$

Two mathematical approaches are available in the model to describe the mineralisation of HSOC: a first order kinetics, as given by Eq. (6) or an approach developed by Wutzler & Reichstein, (2008) and by Guenet *et al.*, (2013) introducing the priming effect, i.e., the mineralisation of HSOC depends on FOC availability, and given by Eq. (7):

$$\frac{\partial HSOC_{t,z,d}}{\partial t} = -k_{HSOC,z} \times HSOC_{t,z,d} \times f_{moist,z} \times f_{temp,z} \quad (6)$$

$$\frac{\partial HSOC_{t,z,d}}{\partial t} = -k_{HSOC,z} \times HSOC_{t,z,d} \times (1 - e^{-PE \times FOC_{t,z,d}}) \times f_{moist,z} \times f_{temp,z} \quad (7)$$

where $HSOC_{t,z,d}$ is the humified SOC carbon pool at a given time (t, in years), depth (z, in m) and distance (d, in m), $k_{HSOC,z}$ is its decomposition rate (yr^{-1}) at a given depth z, and PE is the priming effect parameter. The parameters $f_{moist,z}$ and $f_{temp,z}$ are functions depending respectively on soil moisture and soil temperature at a given depth z, and affecting the decomposition rate of HSOC. They correspond to the moisture equation from Moyano *et al.*, (2012) and to Eq. (3), respectively. The decomposition rate $k_{HSOC,z}$ was an exponential law depending on soil depth (z) as shown by an incubation study (see paragraph *HSOC decomposition rate* further in the M&M):

$$k_{HSOC,z} = a \times e^{-b \times z} \quad (8)$$

The b parameter of this equation represented the ratio of labile C/stable C within the HSOC pool. The effect of clay on HSOC decomposition was implicitly taken into account in this equation as clay content increased with soil depth.

A fraction of decomposed HSOC returns to the FOC assuming that part of the HSOC decomposition products is as labile as FOC (h) and another is respired as CO_2 (Fig. 1a) in the two pools model.

Finally, we also developed an alternative version of the model with three pools by splitting the HSOC pools into two pools with different turnover rates, HSOC2 being more stabilized than HSOC1 (Fig. 1b). The non-respired decomposed FOC is split between HSOC1 and HSOC2 following a parameter f_1. The non-respired decomposed HSOC1 is split between HSOC2 and FOC following a parameter f_2 whereas non-respired decomposed HSOC2 is only redistributed into the FOC pools. The decomposition of HSOC1 and HSOC2 both follow the equation (8) but with different parameter values for a.

2.5.2 Carbon transport mechanisms

The transport of C between the different soil layers was represented by both advection and diffusion mechanisms (Elzein and Balesdent, 1995), which have been shown to usually describe well the C transport in soils (Bruun et al., 2007; Guenet et al., 2013). The advection represents the C transport due to the water infiltration in the soil, while the diffusion represents the C transport due to the fauna activity. The same transport coefficients were applied to the two C pools, FOC and HSOC.

The advection is defined by:

$$F_A = A \times C \qquad (9)$$

where F_A is the flux of *C* transported downwards by advection, and *A* is the advection rate (mm yr^{-1}).

The diffusion is represented by the Fick's law:

$$F_D = -D \times \frac{\partial^2 C}{\partial z^2} \qquad (10)$$

where F_D is the flux of C transported downwards by diffusion, $-D$ the diffusion coefficient (cm^2 yr^{-1}) and *C* the amount of carbon in the pool subject to transport (FOC or HSOC).

To represent the effect of soil tillage ($z \leq 0.2$ m), we added another diffusion term using the Fick's law but with a value of *D* several orders of magnitude higher to represent the mixing due to tillage. It must be noted that no tillage effect on the decomposition was represented here because of the large unknowns on these aspects (Dimassi et al., 2013; Virto et al., 2012).

In this model, the flux of *C* transported downwards by the advection and diffusion (F_{AD}) was represented as the sum of both mechanisms, following Elzein & Balesdent (1995):

$$F_{AD} = F_A + F_D \qquad (11)$$

The FOC and HSOC pools dynamics in the two pools model correspond to:

$$\frac{\partial FOC}{\partial t} = I_{t,z,d} + \frac{\partial F_{AD}}{\partial z} + h \times \frac{\partial HSOC_{t,z,d}}{\partial t} - \frac{\partial FOC_{t,z,d}}{\partial t} \qquad (12)$$

$$\frac{\partial HSOC}{\partial t} = \frac{\partial F_{AD}}{\partial z} + h \times \frac{\partial FOC_{t,z,d}}{\partial t} - \frac{\partial HSOC_{t,z,d}}{\partial t} \qquad (13)$$

Finally, the FOC, HSOC1 and HSOC2 pools dynamics in the three pools model correspond to:

$$\frac{\partial FOC}{\partial t} = I_{t,z,d} + \frac{\partial F_{AD}}{\partial z} + h \times f_2 \times \frac{\partial HSOC1_{t,z,d}}{\partial t} + h \times \frac{\partial HSOC2_{t,z,d}}{\partial t} - \frac{\partial FOC_{t,z,d}}{\partial t} \qquad (14)$$

$$\frac{\partial HSOC1}{\partial t\partial} = \frac{\partial F_{AD}}{\partial z} + h \times f_1 \times \frac{\partial FOC_{t,z,d}}{\partial t} - \frac{\partial HSOC1_{t,z,d}}{\partial t} \qquad (15)$$

$$\frac{\partial HSOC2}{\partial t} = \frac{\partial F_{AD}}{\partial z} + h \times (1 - f_1) \times \frac{\partial FOC_{t,z,d}}{\partial t} + h \times (1 - f_2) \times \frac{\partial HSOC1_{t,z,d}}{\partial t} - \frac{\partial HSOC2_{t,z,d}}{\partial t} \qquad (16)$$

2.5.3 Depth dependence of HSOC potential decomposition rates

The shape of the function (i.e. the *b* parameter) describing the HSOC potential decomposition rate (Eq. (8)) was determined by incubating soils from the control, the alley and the tree row, and from different soil layers (0.0-0.1, 0.1-0.3, 0.7-1.0 and 1.6-1.8 m). Soils were sieved at 5 mm, and incubated during 44 days at 20°C at a water potential of -0.03 MPa. Evolved CO_2 was measured using a micro-GC at 1, 3, 7, 14, 21, 28, 35, 44 days. The three first measurement dates corresponded to a pre-incubation period and were not included in the analysis. For a given depth, the cumulative mineralised SOC was expressed as a percentage of total SOC and was plotted against the incubation time. The slopes represented the potential SOC mineralisation rate at a given soil depth and location. The potential SOC mineralisation rates were then plotted

against soil depth (Fig. S1). We used the soil incubations to determine only the *b* parameter of the curve: with such short term incubations, the SOC decomposition rate over the soil profile is overestimated because the CO_2 measured during the incubations mainly originates from the labile C pool. The *a* parameter was optimized following the procedure described further.

2.6 Boundary conditions of the CARBOSAF model

2.6.1 Annual aggregates of soil temperature and soil moisture

In April 2013, eight soil temperature and moisture sensors (Campbell CS 616 and Campbell 107, respectively) were installed in the agroforestry plot at 0.3, 1.3, 2.8 and 4.0 m depth, and at 2 and 5 m from the trees. Soil temperature and moisture were measured for 11 months.

The mean annual soil temperature in the agroforestry plot was described by the following equation:

$$T = -0.89 \times z + 288.24 \qquad (R^2 = 0.99) \qquad (17)$$

where T is the soil temperature (K) and z is the soil depth (m).

The mean annual soil moisture was described with the following equation:

$$\theta = 0.05 \times z + 0.28 \qquad (R^2 = 0.99) \qquad (18)$$

where θ is the soil volumetric moisture (cm cm^{-3}) and z is the soil depth (m).

Due to a lack of data in the agricultural plot, we assumed that the soil temperature and the soil moisture were the same in the agroforestry tree rows, alleys and in the control plot, but we further performed a sensitivity analysis of the model on these two parameters.

2.6.2 Interpolation of tree growth

The tree growth has been measured in the field since the establishment of the experiment. We used the diameter at breast height (*DBH*) as a surrogate of the tree growth preferentially to the

tree height as the field measurements were more accurate. Indeed, *DBH* is easier to measure than height, especially when trees are getting older. To describe the temporal dynamic of *DBH* since the tree planting, a linear equation was fitted on the data.

Tree growth measurements enabled us to fit the following equation that was used in the model:

$$DBH_t \begin{cases} 0.01, & t \leq 3 \\ 0.0157 \times t - 0.0391 \ (R^2 = 0.997) & 3 < t \leq 20 \end{cases} \quad (19)$$

where DBH_t is the diameter at breast height (m) and t represents the time since tree planting (years).

2.6.3 Change of tree litterfall over time

For the five walnut trees where the leaf biomass was quantified, *DBH* was also measured. The ratio between the leaf biomass and *DBH* was then calculated for the five replicates. Total leaf biomass was 8.96 ± 1.45 kg DM tree^{-1} and the carbon concentration of walnut leaves was 449.4 ± 3.7 mg C g^{-1} (Table 2). With a density of 110 trees ha^{-1}, leaf litterfall was estimated at 0.73 ± 0.06 t C ha^{-1} in 2012 and at the plot scale. The ratio between leaf biomass and *DBH* was 0.0277 ± 0.0024 t C tree^{-1} m^{-1} or 3.05 t C ha^{-1} m^{-1}. The following linear relationship was therefore used in the model to describe leaf litter C input with the tree growth:

$$L_t = 3.05 \times DBH_t \quad (20)$$

where L_t is the leaf litter input (t C ha^{-1}) at the year t, and DBH_t the diameter at breast height (m) the year t.

2.6.4 Tree fine root C input from mortality

In 2012, the measured tree fine root biomass was higher in the tree row than in the alley (Table S1). From 0 to 1 m distance from the tree (in the tree row), the tree fine root biomass was homogeneous and was 1.01 t C ha^{-1} down 2 m depth.

In 2012 and in the alley, the tree fine root biomass (*TFRB*) decreased with increasing distance from the tree and was represented by an exponential function:

$$TFRB = \begin{cases} 1.01, & 0 \le d \le 1 \\ 1.29 \times e^{-0.28 \times d} \quad (R^2 = 0.90), & 1 < d \le 6.5 \end{cases} \qquad (21)$$

where *TFRB* represents tree fine root biomass down 2 m depth (t C ha^{-1}), and *d* the distance from the tree (m).

We considered a linear increase of *TFRB* with increasing *DBH*, and a linear regression was performed between *TFRB* in 2012 and *TFRB* in 1996, the first year after planting (biomass considered as negligible). The following linear relationship was used to simulate *TFRB* as a function of tree growth:

$$TFRB_{t,d} = \begin{cases} 3.69 \times DBH_t, & 0 \le d \le 1 \\ 4.70 \times DBH_t \times e^{-0.28 \times d}, & 1 < d \le 6.5 \end{cases} \qquad (22)$$

where $TFRB_t$ represents the tree fine root biomass to 2 m depth (t C ha^{-1}) at the year *t*, DBH_t the diameter at breast height (m) at the year *t*, and *d* the distance to the tree (m).

A changing distribution of tree fine roots within the soil profile was taken into account with increasing distance to the tree. For this purpose, exponential functions ($a \times e^{-b \times z}$) were fitted in the alley every 0.5 m distance, and a linear regression was fitted between their coefficients *a* and *b* and distance from the tree. However, the distribution of *TFRB* within the soil profile and with the distance to the tree was considered constant with time.

A decreasing exponential function best represented the changing distribution of tree fine roots within the soil profile with increasing distance to the tree:

$$p_{TFRB,z,d} = \begin{cases} 13.92 \times e^{-1.39 \times z} \quad (R^2 = 0.68), & 0 \le d \le 1 \\ a \times e^{-b \times z}, & 1 < d \le 6.5 \end{cases} \qquad (23)$$

and

$$a = 10.31 - 1.15 \times d \quad (R^2 = 0.69) \qquad (24)$$

$$b = -1.10 + 0.19 \times d \quad (R^2 = 0.51) \qquad (25)$$

Finally,

$$p_{TFRB,z,d} = \begin{cases} 13.92 \times e^{-1.39 \times z}, & 0 \le d \le 1 \\ (10.31 - 1.15 \times d) \times e^{-(-1.10 + 0.19 \times d) \times z}, & 1 < d \le 6.5 \end{cases} \qquad (26)$$

where $p_{TFRB,z,d}$ is the proportion (%) of the total tree fine root biomass (*TFRB*) at a given depth *z* (m), and at a distance *d* from the tree (m).

To finally estimate the tree fine root input due to the mortality, *TFRB* was multiplied by the measured root turnover. The tree fine root turnover ranged from 1.7 to 2.8 yr^{-1} depending on fine root diameter, with an average turnover of 2.2 yr^{-1} for fine roots ≤ 2 mm and to a depth of 2 m (Germon et al., 2016).

2.6.5 Aboveground and belowground input from the crop

As there were more crop yield measurements (14) than straw biomass measurements (6), the effect of agroforestry on the crop yield with time was used as an estimate for change in the aboveground and belowground wheat biomass.

For this, the relative yield ($Rel\ Y_{AF}$) in the agroforestry system was calculated for each year as the ratio between the agroforestry yield and the control yield (Y_C).

The average annual crop yield in the control plot was $Y_C = 3.79 \pm 0.40$ t DM ha^{-1} for the 14 studied years. In the agroforestry plot, the average relative yield decreased linearly with time (increasing *DBH*) and was described using the following linear equation (Fig. 2):

$$Rel\ Y_{AF_t} = -93.33 \times DBH_t + 100 \qquad (R^2 = 0.12, \quad p - value = 0.02) \qquad (27)$$

where $Rel\ Y_{AF_t}$ is the average relative crop yield (%) in the agroforestry plot compared to the control plot at year *t*, and DBH_t is the diameter at breast height (m) at year *t*.

The variation of crop yield with distance from the trees was described with a quadratic equation (Fig. 2). But as we aimed to predict SOC stocks up to 6.5 m distance from the trees (middle of the alley), a linear increase of crop yield with increasing distance from the tree gave similar results as the quadratic equation over the 6.5 m distance and was more parsimonious:

$$Rel\,Y_{AF_d} = 4.39 \times d + 64.57 \quad (R^2 = 0.24), \qquad 1 < d \leq 6.5 \qquad (28)$$

where $Rel\,Y_{AF_d}$ is the relative crop yield (%) in the agroforestry plot at a distance d (m) from the tree compared to the control plot.

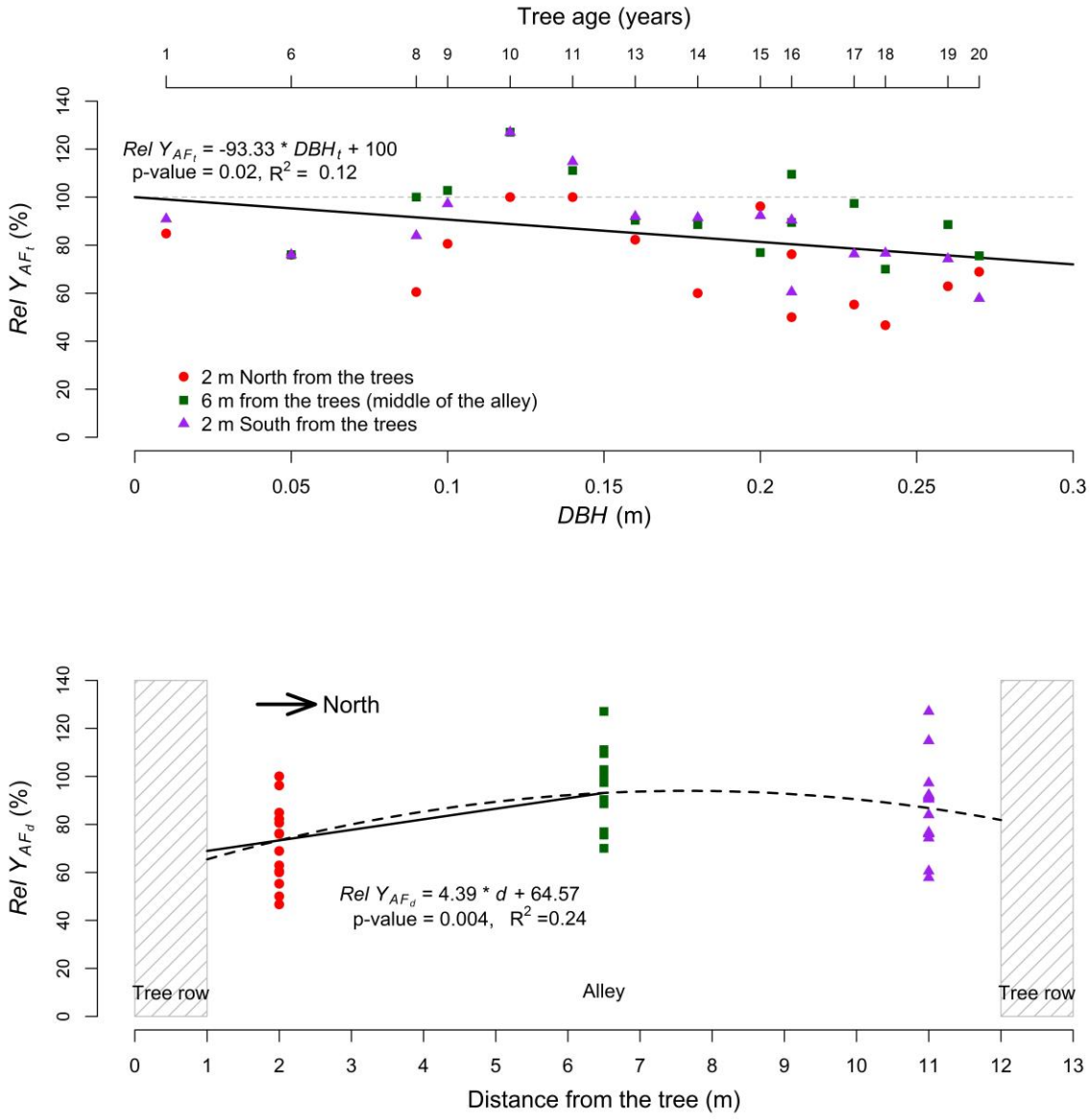

Fig. 2. Top: Relative yield ($Rel\ Y_{AF_t}$) in the agroforestry plot compared to the control plot as a function of tree growth, represented by the diameter at breast height (*DBH*) at year *t*. Bottom: Relative yield ($Y_{AF_{t,d}}$) as a function of the distance from the tree.

Finally, the crop yield in the agroforestry plot was modeled as follows:

$$Y_{AF_{t,d}} = Rel\ Y_{AF_t} \times\ Y_C\ \times Rel\ Y_{AF_d} \quad (R^2 = 0.19), \qquad 1 < d \leq 6.5 \qquad (29)$$

where $Y_{AF_{t,d}}$ is the crop yield (t DM ha^{-1}) in the agroforestry plot at the year *t* and at a distance *d* (m) from the tree. Because three linear equations were used to describe the crop yield in the agroforestry plot, errors were accumulated and we finally came up with a standard underestimation of the crop yield in the agroforestry plot that we corrected by multiplying our equation by 1.2.

The ratio between the straw biomass and the crop yield was calculated as the average of the six measurements, and was considered constant with time. This ratio was used to convert crop yield into straw biomass. In the agroforestry plot, the carbon input to the soil from the aboveground crop biomass was:

$$ABC_{crop,t,d} = Y_{AF_{t,d}} \times (straw\ biomass{:}\ crop\ yield)\ \times\ C_{straw}\ \times\ (1 - export) \qquad (30)$$

where $ABC_{crop,t,d}$ is the aboveground carbon input from the crop (t C ha^{-1}) at the year *t* and distance *d* from the tree, $Y_{AF_{t,d}}$ is the agroforestry crop yield. The average ratio between the straw biomass (t DM ha^{-1}) and the crop yield (t DM ha^{-1}) equaled 1.03 ± 0.11 (n=6). The wheat straw was exported out of the field after the harvest, but it was estimated that 25% of the straw biomass was left on the soil, thus *export*=0.75. In the control plot, $Y_{AF_{t,d}}$ was replaced by Y_C.

To estimate fine root biomass of the crop, we hypothesized that the root:shoot ratio of the durum wheat was the same in both the agroforestry and agricultural plot, in the absence of any

published data on the matter. In the agroforestry plot, the belowground crop biomass was represented by:

$$BEC_{crop,t,d} = Y_{AF_{t,d}} \times (shoot{:}\, crop\ yield) \times (root{:}\, shoot) \times C_{root} \quad (31)$$

where $BEC_{crop,t,d}$ is the belowground crop biomass (t C ha^{-1}) at the year t and at a distance d from the tree, $Y_{AF_{t,d}}$ is the agroforestry crop yield. The average ratio between the total crop aboveground biomass (*shoot*) and the crop yield equaled 2.45 ± 0.15 (n=6). In 2012, total fine root biomass was 2.29 ± 0.32 t C ha^{-1} in the control (Table 3).

Table 3. Wheat fine root biomass in the agricultural control plot in 2012.

Soil depth (m)	Wheat fine root biomass (kg C m^{-3})	(t C ha^{-1})
0.0-0.1	0.48 ± 0.05	0.48 ± 0.05
0.1-0.3	0.34 ± 0.04	0.69 ± 0.09
0.3-0.5	0.22 ± 0.04	0.44 ± 0.08
0.5-1.0	0.10 ± 0.04	0.52 ± 0.20
1.0-1.5	0.03 ± 0.04	0.17 ± 0.19
Total	-	2.29 ± 0.32

Errors represent standard errors.

Therefore, the wheat *root:shoot* ratio equaled 0.79 ± 0.12 (n=1). The carbon concentration of wheat root was C_{root} = 35.14 ± 1.90 mg C g^{-1}. In the control plot, $Y_{AF_{t,d}}$ was replaced by Y_C.

In 2012, no wheat roots were observed below 1.5 m, and root biomass decreased exponentially with increasing depth (Table 3). The distribution of crop roots within the soil profile was described as follows:

$$p_{CRBc,z} = \begin{cases} 26.44 \times e^{-2.59 \times z} & (R^2 = 0.99), \quad z \le 1.5 \\ 0, & z > 1.5 \end{cases} \quad (32)$$

where $p_{CRBc,z}$ is the proportion (%) of total crop root biomass in the control plot at a given depth z (m).

Since the same maximum rooting depth of the crop was observed in the agroforestry plot and in the control plot, we inferred that the wheat root distribution within the soil profile was not modified by agroforestry, but only its biomass. The crop root turnover was assumed to be 1 yr^{-1}, root mortality occurring mainly after crop harvest.

2.6.6 Aboveground and belowground input from herbaceous vegetation in the tree rows

The distance from the trees had no effect on the above and belowground biomass of the herbaceous vegetation (data not shown), therefore average values are presented. The summer aboveground biomass was almost three times higher than in winter, whereas the belowground biomass was two times higher (Table 4). The total aboveground carbon input was 2.13 ± 0.14 t C ha^{-1} yr^{-1} and the total belowground carbon input was 0.74 ± 0.05 t C ha^{-1} yr^{-1} to 0.5 m depth.

Table 4. Aboveground and belowground biomass of the herbaceous vegetation in the tree rows.

		Herbaceous biomass (t C ha^{-1})	
	Soil depth (m)	Summer	Winter
Aboveground	-	1.57 ± 0.11	0.56 ± 0.09
Belowground	0.0-0.1	0.22 ± 0.03	0.17 ± 0.01
	0.1-0.3	0.16 ± 0.02	0.06 ± 0.01
	0.3-0.5	0.09 ± 0.04	0.04 ± 0.01
	Total	0.46 ± 0.04	0.27 ± 0.02

Errors represent standard errors.

The belowground carbon input from the tree row vegetation ($BEC_{veg,z}$, t C ha^{-1}) at a given depth z (m) was described by the following equation:

$$BEC_{veg,z} = \begin{cases} 0.44 \times e^{-3.12 \times z}, & z \leq 1.5 \\ 0, & z > 1.5 \end{cases} \quad (33)$$

We assumed for simplification that the aboveground and belowground biomasses of the herbaceous vegetation in the tree row were constant over time.

2.7 Optimization procedure

Depending on the model variant, four to five parameters were optimized with a Bayesian statistical method (Santaren et al., 2007; Tarantola, 1987, 2005) using measured SOC stocks from the control plot only. These parameters were *A*, the advection rate, *D*, the diffusion coefficient, *h* the humification yield, *a* the coefficient of the k_{HSOC} rate from Eq. (10), and *PE* the priming coefficient. These four or five parameters were calibrated so that equilibrium SOC stocks, i.e. after 5000 years of simulation, equaled SOC stocks of the control plot in 2013. The associated uncertainty was estimated with the 93 soil cores sampled in the control plot (see section 2.2.1). Due to a lack of relevant data, we assumed that the climate and the land use were the same for the last 5000 years, and that SOC stocks in the control plot were at equilibrium at the time of measurement. Therefore, SOC stocks at the end of the 5000 years of simulation equaled SOC stocks in the control plot. Three different calibrations were performed, corresponding to the three different models that were used: one calibration with the two pools model without the priming effect, one calibration with the two pools model with the priming effect, and one calibration with the three pools model.

Each model variant was fitted to the control SOC stocks data using a Bayesian curve fitting method described in Tarantola (1987), after a conversion from SOC stocks in kg C m^{-2} to SOC stocks in kg m^{-3} due to the different soil layers' thickness. We aimed to find a parameter set that minimizes the distance between model outputs and the corresponding observations, considering model and data uncertainties, and prior information on parameters. With the assumption of Gaussian errors for both the observations and the prior parameters, the optimal parameter set corresponds to the minimum of the cost function $\boldsymbol{J}(\boldsymbol{x})$:

$$\boldsymbol{J}(\boldsymbol{x}) = 0.5 \times \left[(\boldsymbol{y} - \boldsymbol{H}(\boldsymbol{x}))^t \times \boldsymbol{R}^{-1} \times \left(\boldsymbol{y} - \boldsymbol{H}(\boldsymbol{x})\right) + (\boldsymbol{x} - \boldsymbol{x}_b)^t \times {\boldsymbol{P}_b}^{-1} \times (\boldsymbol{x} - \boldsymbol{x}_b)\right] \quad (34)$$

that contains both the mismatch between modelled and observed SOC stock and the mismatch between a priori and optimized parameters. $\boldsymbol{x}$ is the vector of unknown parameters, $\boldsymbol{x}_b$ the vector of a priori parameter values, $\boldsymbol{H()}$ the model and y the vector of observations. The covariance matrices $\boldsymbol{P}_b$ and $\boldsymbol{R}$ describe a priori uncertainties on parameters, and observations, respectively. Both matrices are diagonal as we suppose the observation uncertainties and the parameter uncertainties to be independent. To determine an optimal set of parameters which minimizes $\boldsymbol{J}(\boldsymbol{x})$, we used the BFGS gradient-based algorithm (Tarantola, 1987). For each model variant, we performed 30 optimizations starting with different parameter prior values to check that the results did not correspond to a local minimum. As the BFGS algorithm does not directly calculate the variance of posteriors, they were quantified using the curvature cost function at its minimum once it was reached (Santaren et al., 2007).

2.8 Comparison of models

Model predictions with and without priming effect were compared calculating the coefficients of determination, root mean square errors (RMSE) and Bayesian information criteria (BIC).

$$RMSE = \sqrt{\frac{1}{N}\sum_{i=1}^{N}(x_i - \bar{x})^2} \qquad (35)$$

where i is the number of observations (1 to N), x_i is the predicted value and $\bar{x}$ is the mean observed value.

$$BIC = N \times \ln(MSD) + k \times \ln(N) \qquad (36)$$

where N is the number of observations, MSD is the mean squared deviation used to estimate the maximum likelihood (Manzoni et al., 2012), and k is the number of model parameters.

588 The model was run at a yearly time step using mean annual soil temperature and moisture and
589 annual C inputs to the soil. In the agroforestry, the model was run from the ground (0 m) to 2
590 m depth, and from the tree (0 m) to 6.5 m from the tree (middle of the alley). The model was
591 applied separately across locations of a tree-distance gradient having varying OC inputs, each
592 soil column was considered independent from another. SOC pools were initialized after a spin-
593 up of 5000 years in the control plot. At t_0, SOC stocks in the agroforestry plot therefore equaled
594 SOC stocks of the control plot. The model was then run from t_0 to t_{18} (years) after tree planting.
595 The spatial resolution was 0.1 m both vertically and horizontally. The model was developed
596 using R 3.1.1 (R Development Core Team, 2013). Partial-differential equations were solved
597 using the R package *deSolve* and the *ode.1D* method (Soetaert et al., 2010).
598
599 **2.9 Estimation of the priming intensity and its impact on SOC storage**
600 In equation (7), the priming effect (*PE*) is considered as a control of the FOC on the HSOC
601 decomposition and not as an accelerating factor of the HSOC decomposition. This method
602 followed the Wutzler & Reichstein, (2008) approach based on the microbial biomass and
603 adapted to the FOC by Guenet *et al.*, (2013) for models without explicit microbial biomass.
604 Models able to reproduce priming effect generally need an explicit microbial biomass
605 controlling the decomposition (Blagodatsky et al., 2010; Perveen et al., 2014). The priming
606 scheme used here allows some simplifications in the model structure since an explicit
607 representation of the microbial biomass is not needed. Furthermore, at equilibrium state (i.e.
608 when the input rate is constant) the decomposition rate of a first order equation (Eq. (6)) takes
609 *PE* implicitly into account. Indeed, when FOC enters the system, there is an induced priming,
610 a constant FOC input rate therefore induces a constant priming. This means that when we
611 optimized the decomposition rate parameter in the control plot, we implicitly represented this
612 priming but at a fixed rate. When FOC inputs are modified, due to the tree growth for instance,

613 the *PE* intensity is modified and this effect cannot be represented by classical first order
614 kinetics. To estimate the importance of priming on SOC storage in the agroforestry plot, the
615 simulations using first order equations (Eq. (6)) can therefore not be directly compared to the
616 simulations using the FOC-dependant decomposition rate (Eq. (7)). To estimate the change of
617 SOC decomposition rate due to priming when trees are planted, the decomposition fluxes
618 predicted by Eq. (7) $\left(-k_{HSOC,z} \times (1 - e^{-PE \times FOC_{t,z,d}})\right)$ in the agroforestry plot must be
619 compared to the fluxes in the agroforestry plot using the decomposition rate from the control
620 plot calculated by Eq. (7) with $FOC_{t,z,d}$ corresponding to the FOC inputs in the control plot.
621 Thus, to calculate the importance of priming on SOC storage when trees are planted, we used
622 the decomposition rates calculated following Eq. (7) in the control plot $\left(-k_{HSOC,z} \times\right.$
623 $\left.(1 - e^{-PE \times FOC_{t,z,d}})\right)$ and we applied this decomposition rate to the agroforestry plot as a
624 classical first order kinetics (without the control FOC, i.e. $k_{new} = -k_{HSOC,z} \times (1 -$
625 $e^{-PE \times FOC_{t,z,d}}$) with $FOC_{t,z,d}$ fixed constant). This simulation corresponded to the absence of
626 priming due to trees in the agroforestry plot (i.e. decomposition not controlled by the FOC of
627 the agroforestry plot). By difference with the simulation performed with the full two pools
628 model (Eq. (7)), i.e., taking account of FOC input and priming, we calculated the priming
629 intensity.
630
631 **3 Results**
632 **3.1 Organic carbon inputs and SOC stocks: a synthesis from field measurements**
633 Tree rows in the agroforestry system received two times more organic carbon (OC) inputs
634 compared to the control plot (Fig. 3), and 65% more than alleys. Overall, the agroforestry plot
635 had 41% more OC inputs to the soil than the control plot to 2 m depth (3.80 t C ha^{-1} yr^{-1}
636 compared to 2.69 t C ha^{-1} yr^{-1}). In the agroforestry plot, the largest aboveground OC input to

the soil comes from the herbaceous vegetation, and not from the trees. In the control plot, 85% of OC inputs are wheat root litters. In the agroforestry plot, root inputs represent 71% of OC inputs in the alleys, and 50% in the tree rows.

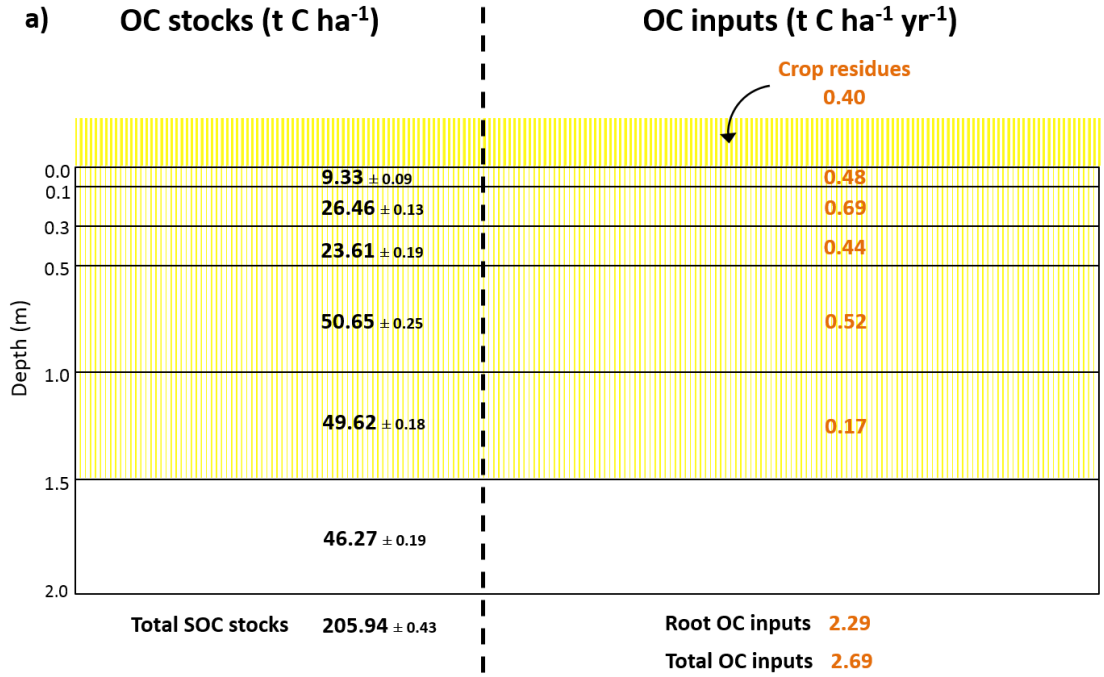

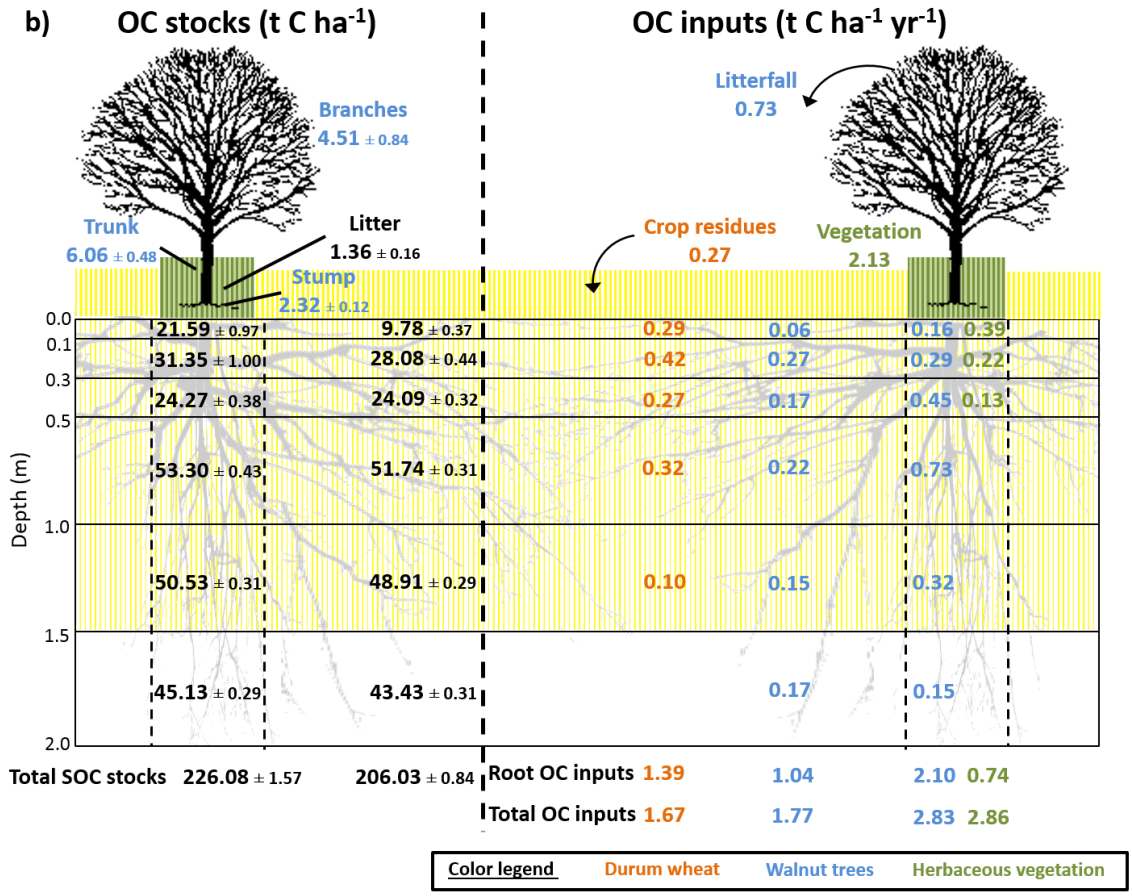

Fig. 3. Measured soil organic carbon stocks and organic carbon inputs to the soil a) in the agricultural control plot, b) in the 18-year-old agroforestry plot. Associated errors are standard errors. Values are expressed per hectare of land type (control, alley, tree row). To get the values per hectare of agroforestry, data from alley and tree row have to be weighted by their respective surface area (i.e., 84% and 16%, respectively) and then added up. OC: organic carbon; SOC: soil organic carbon. SOC stocks data are issued from Cardinael *et al.*, (2015a), data of tree root OC inputs are combined from Cardinael *et al.*, (2015b) and from Germon *et al.*, (2016).

3.2 HSOC decomposition rate

The soil incubation experiment showed that the HSOC mineralization rate decreased exponentially with depth (Fig. S1) and could be described with:

$$k_{HSOC,z} = 6.114 \times e^{-1.37 \times z} \quad (R^2 = 0.76) \qquad (34)$$

where z is the soil depth (m), and where the a (yr^{-1}) coefficient (a = 6.114) was further optimized (Table 5).

Table 5. Summary of optimized model parameters.

Model parameter	Meaning	Prior range	Posterior values ± variance (prior values)		
			2 pools - without *PE*	2 pools - with *PE*	3 pools – without *PE*
a	coefficient from Eq. (8) of the HSOC decomposition (yr^{-1})	$3.65e^{-6}$-3.65	$0.01e^{-2} \pm <10^{-4}$ ($0.01e^{-2}$)	$0.01e^{-2} \pm <10^{-4}$ ($0.01e^{-2}$)	-
a_1	coefficient from Eq. (8) of the HSOC1 decomposition (yr^{-1})	$3.65e^{-6}$-3.65	-	-	$0.01e^{-2} \pm <10^{-4}$ ($0.01e^{-2}$)
a_2	coefficient from Eq. (8) of the HSOC2 decomposition (yr^{-1})	$3.65e^{-6}$-3.65	-	-	$0.83e^{-2} \pm 0.17e^{-2}$ ($0.83e^{-2}$)
D	diffusion coefficient ($cm^2\ yr^{-1}$)	$1e^{-6}$-1	$4.62e^{-4} \pm 5.95e^{-4}$ ($9.64e^{-4}$)	$5.63e^{-4} \pm 1.42e^{-4}$ ($9.01e^{-4}$)	$5.24e^{-4} \pm 7.62e^{-4}$ ($9.64e^{-4}$)
A	advection rate ($mm\ yr^{-1}$)	$1e^{-6}$-1	$21.25e^{-4} \pm 5.02e^{-4}$ ($8.54e^{-4}$)	$6.63e^{-4} \pm 2.38e^{-4}$ ($4.27e^{-4}$)	$21.60e^{-4} \pm 2.24e^{-4}$ ($8.54e^{-4}$)
h	humification yield	0.01-1	$0.32 \pm <10^{-4}$ (0.34)	$0.25 \pm 1.00e^{-4}$ (0.13)	0.34 ± 0.03 (0.34)
PE	priming coefficient	0.1-160	-	9.66 ± 1.49 (102.95)	-
f_1	fraction of decomposed FOC entering the HSOC1 pool	0-1	-	-	0.99 ± 0.18 (0.86)
f_2	fraction of decomposed HSOC1 entering the FOC pool	0-1	-	-	$0.94 \pm 1.10e^{-3}$ (0.80)

The prior range represents the range in which prior values were sampled for the 30 optimizations per model variant. The prior values presented in brackets in the posterior column represent the prior values that minimized the **J(x)** value (Eq. (34)).

663 **3.3 Modeling results**

664 **3.3.1 Optimized parameters and correlation matrix**

665 The optimized parameters and their prior modes are presented in Table 5. For the two pools
666 model without priming effect, the most important correlation was observed between *h* and *A*
667 which control the humification and the transport by advection. Concerning the two pools model
668 with priming effect, the most important correlations were observed between *h* and *PE* which
669 controls the effect of the FOC on HSOC decomposition, and between *h* and *A*. *A* and *PE* were
670 also positively correlated (Fig. S2). For the three pools model, f_1 and f_2 were by definition
671 negatively correlated, but f_2 and *A* were also correlated. Considering the method used to
672 optimize the parameters, these important correlation factors hinder the presentation of the
673 model output within an envelope. Therefore, we presented the model results using the optimized
674 parameter without any envelope.

675

676 **3.3.2 Modeled SOC stocks**

677 As a reminder, SOC stocks of the agroforestry plot were not part of model calibration (that used
678 the control plot only) but were used here for validation. Observed SOC stocks were not well
679 represented by the two pools model without priming effect, with RMSE ranging from 1.00 to
680 1.07 kg C m^{-3} (Fig. 4, Table S2). The model performed better when the priming effect was
681 taken into account, with RMSE ranging from 0.41 to 0.95 kg C m^{-3}, and the SOC profile was
682 well described. The representation of SOC stocks was not improved by the inclusion of a third
683 C pool in the model. Overall, the two pools model with priming effect was the best one, as
684 shown by the BICs (Fig. 4, Table S2). For all models, SOC stocks below 1 m depth were better
685 described than above SOC stocks (Table S2). The spatial distribution of SOC stocks and of
686 additional SOC storage was also well described (Fig. 5), with a very high additional SOC
687 storage in the topsoil layer in the tree row. Most modeled SOC storage in the agroforestry plot

688 was located in the first 0.2 m depth, but SOC storage was slightly higher in the middle of the
689 alleys than in the alleys close to the tree rows.

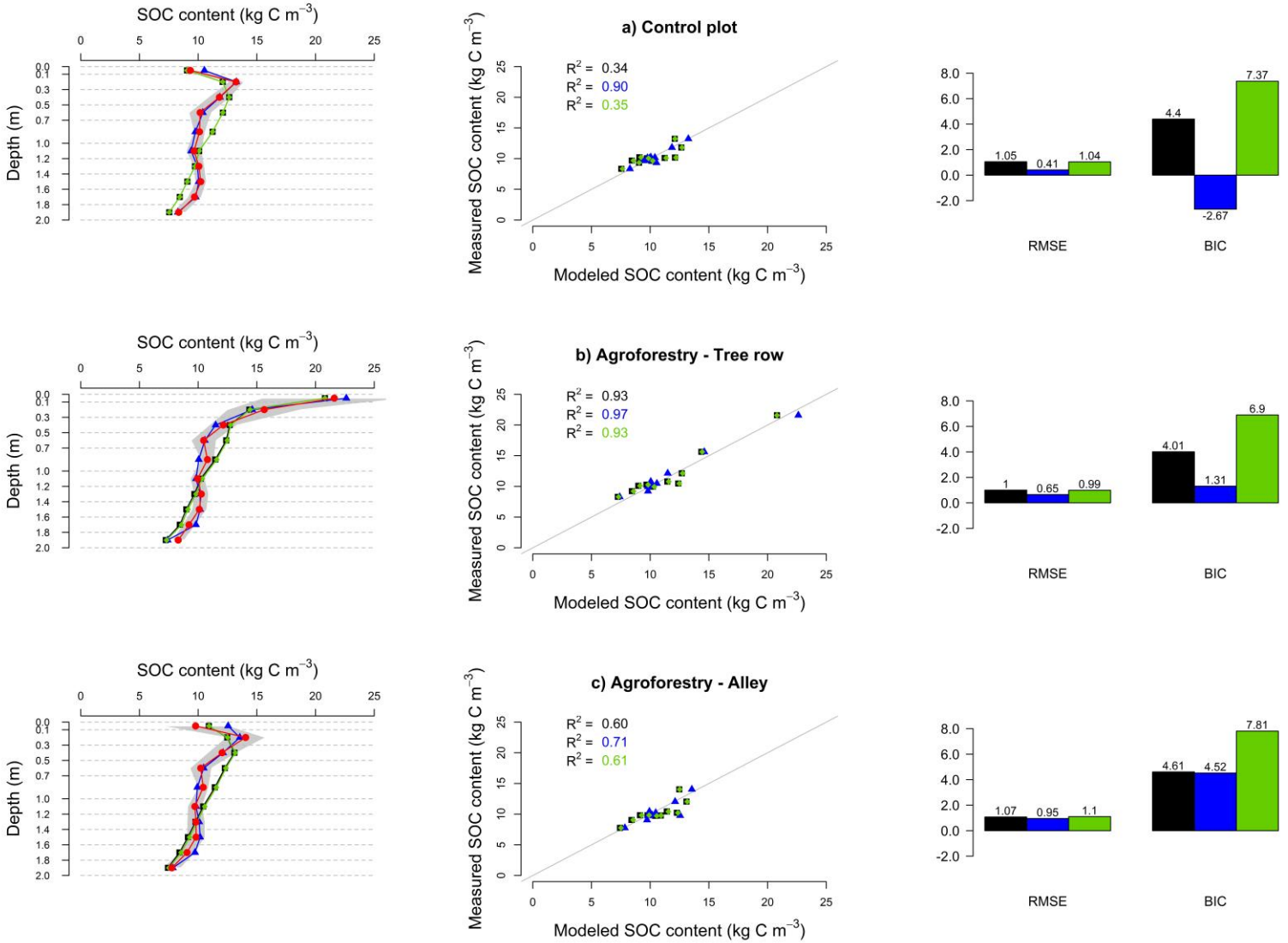
SOC content (kg C m^{-3})
Depth (m)
a) Control plot
R^2 = 0.34
R^2 = 0.90
R^2 = 0.35
Measured SOC content (kg C m^{-3})
Modeled SOC content (kg C m^{-3})
1.05
0.41
1.04
4.4
-2.67
7.37
RMSE
BIC
b) Agroforestry - Tree row
R^2 = 0.93
R^2 = 0.97
R^2 = 0.93
1
0.65
0.99
4.01
1.31
6.9
c) Agroforestry - Alley
R^2 = 0.60
R^2 = 0.71
R^2 = 0.61
1.07
0.95
1.1
4.61
4.52
7.81
Modeled / 2 pools - no PE
Modeled / 2 pools - PE
Modeled / 3 pools - no PE
Measured

690

Fig. 4. Measured and modeled soil organic carbon contents (kg C m^{-3}) in an agricultural control plot and in an 18-year-old silvoarable system with a two pools model without priming effect (no *PE*), with a two pools model with priming effect (*PE*) and with a three pools model without *PE*. Gray shaded bands represent standard deviations of measured SOC stocks (n=93 in the control, n=40 in the tree rows, and n=60 in the alleys).

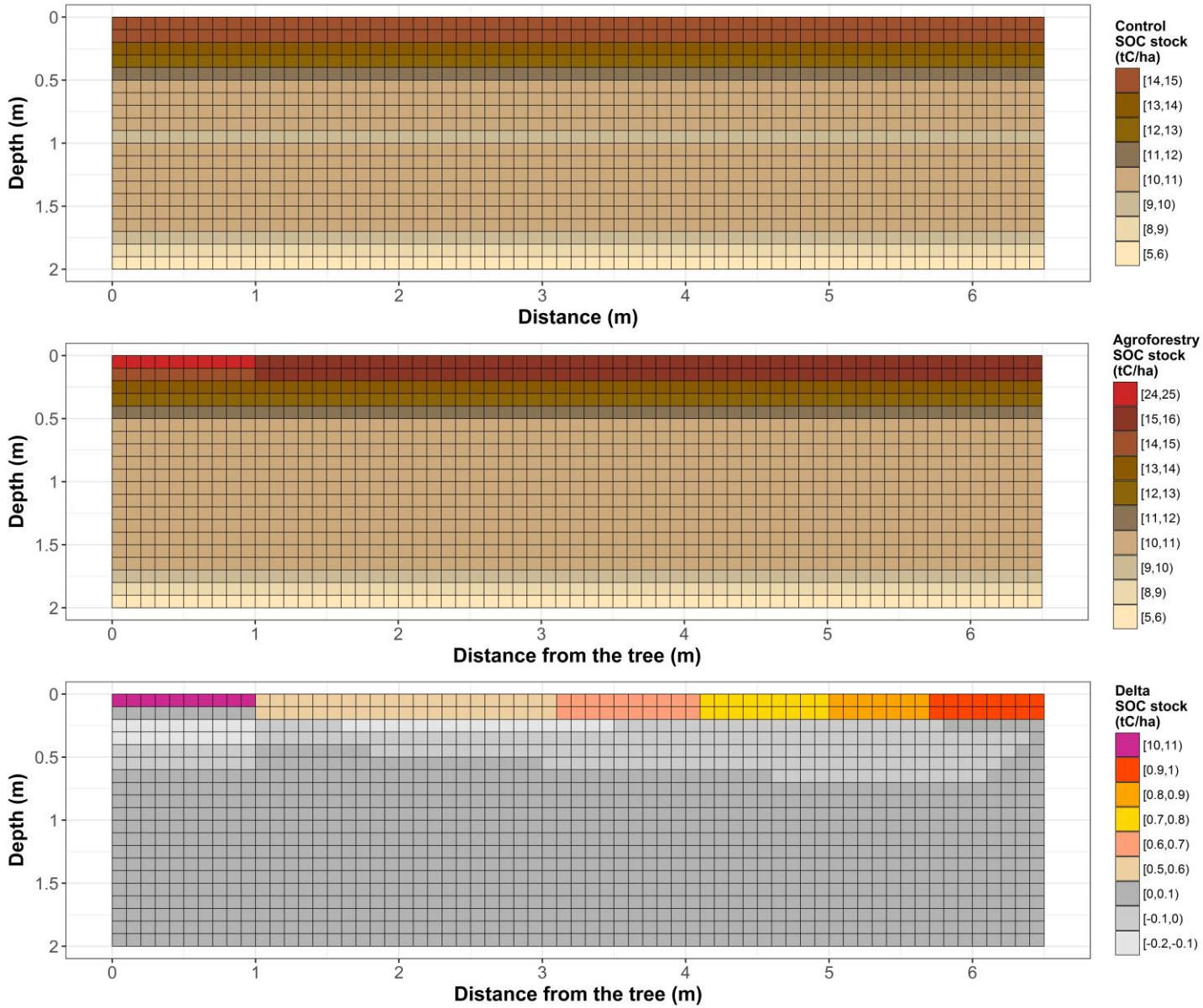
Depth (m)
Distance (m)
Control SOC stock (tC/ha)
[14,15)
[13,14)
[12,13)
[11,12)
[10,11)
[9,10)
[8,9)
[5,6)
Distance from the tree (m)
Agroforestry SOC stock (tC/ha)
[24,25)
[15,16)
[14,15)
[13,14)
[12,13)
[11,12)
[10,11)
[9,10)
[8,9)
[5,6)
Distance from the tree (m)
Delta SOC stock (tC/ha)
[10,11)
[0.9,1)
[0.8,0.9)
[0.7,0.8)
[0.6,0.7)
[0.5,0.6)
[0,0.1)
[-0.1,0)
[-0.2,-0.1)

702

Fig. 5. Spatial distribution of control SOC stocks (top), agroforestry SOC stocks (middle), and additional SOC storage (t C ha^{-1}) in an 18-year-old silvoarable system compared to an agricultural control plot and represented by the two pools model with priming effect.

3.3.3 Antagonist effect of priming on SOC storage

The priming effect increases the decomposition rate when more FOC is available (Fontaine et al., 2007). Therefore, the effect of a C inputs increase on SOC storage in the agroforestry plot might be counterbalanced by priming. With our model we were able to estimate the contribution of each driver on SOC storage. The introduction of priming effect in the model reduced the potential SOC storage due to higher organic inputs in the agroforestry system by 91% in the alley, and by 76% in the tree rows (Fig. 6). The potential effect of OC inputs alone on SOC storage was 49.12 to 62.77 t C ha^{-1}, but the effect of priming on SOC storage was -44.89 to -47.67 t C ha^{-1}, resulting in a modeled SOC storage of 4.23 t C ha^{-1} in the alley and of 15.09 t C ha^{-1} in the tree row down 2 depth (Fig. 6). The negative effect of priming effect on SOC storage increased with increasing soil depth (Fig. S3).

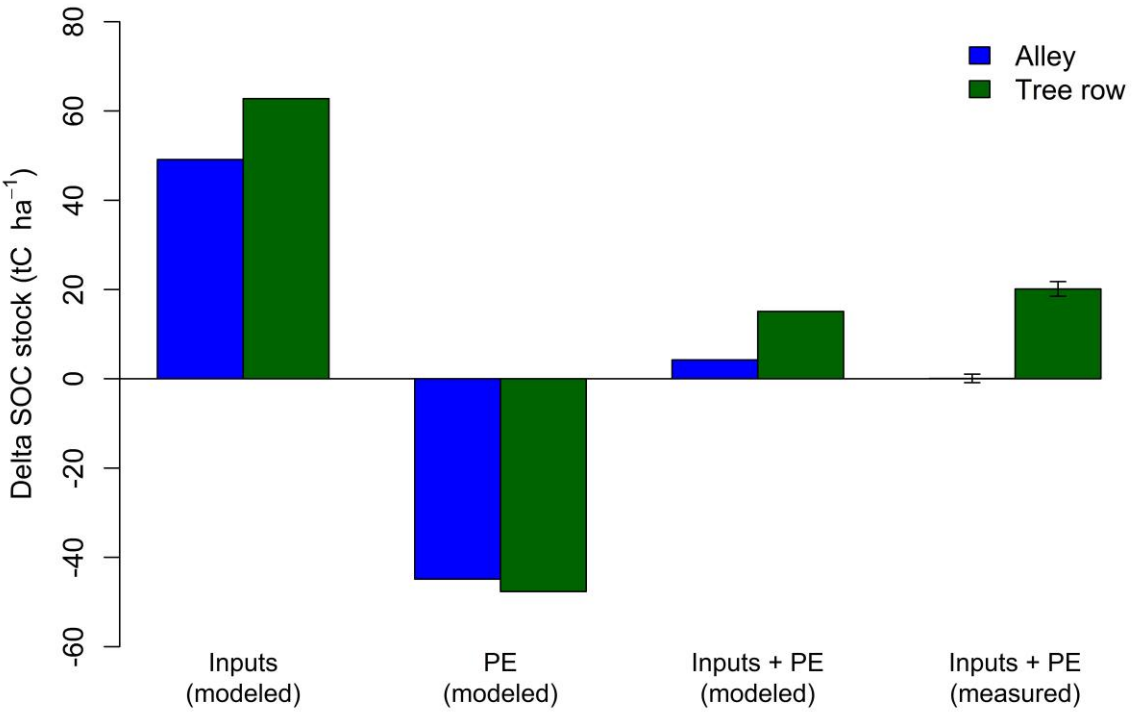

Fig. 6. Decoupling the role of C inputs and priming effect (*PE*) on SOC storage in an 18-year-old silvoarable system down 2 m depth. Inputs: only the input effect is modeled; *PE*:

only the priming effect is modeled; Inputs + *PE*: model prediction with both processes taken into account.

4 Discussion

4.1 OC inputs drive SOC storage in agroforestry systems

Increased SOC stocks in the agroforestry plot compared to the control may be explained either by increased OC inputs, or decreased OC outputs by SOC mineralization, or both. Measured organic carbon inputs to soil were increased by 40% down to 2m depth in the 18-year-old agroforestry plot compared to the control plot. Increased OC inputs in agroforestry systems has been shown in other studies but they were only quantified in the first 20 cm of soil (Oelbermann et al., 2006; Peichl et al., 2006). This study is therefore the first one also quantifying deep OC inputs to soil. In this study and due to a lack of data, soil temperature and soil moisture were considered the same in both plots so that abiotic factors controlling SOC decomposition were identical. Despite these simplifying assumptions on similarities in microclimate but also on vertical transport between the control and the agroforestry system, the model calibrated to the control plot was able to reproduce SOC stocks in tree rows and alleys and its depth distribution well. This strong validation also suggests that OC inputs is the main driver of SOC storage at this site, and that a potential effect of agroforestry microclimate on SOC mineralization is of minor importance. Reduced soil temperature is often observed in agroforestry systems (Clinch et al., 2009; Dubbert et al., 2014), but effect of agroforestry on soil moisture is much more complex. The soil evaporation is reduced under the trees, but water is lost through their transpiration (Ilstedt et al., 2016; Ong and Leakey, 1999), and these effects vary with the distance from the tree (Odhiambo et al., 2001). Moreover, the water infiltration and the water storage can be increased under the trees after a rainy event (Anderson et al., 2009). Therefore, the effect of agroforestry on soil moisture is variable in time and space, and should be

744 investigated more in details. Interactions between soil temperature and soil moisture on the
745 SOC decomposition are known to be complex (Conant et al., 2011; Moyano et al., 2013; Sierra
746 et al., 2015) and up to now it is not possible to predict the effect of agroforestry microclimate
747 on the SOC decomposition rate. A sensitivity analysis performed on these two boundary
748 conditions showed that the model was not very sensitive to soil temperature and soil moisture
749 (Fig. S4), but the real effect of these two parameters on SOC dynamics under agroforestry
750 systems should be better investigated in future studies. Furthermore, the SOC decomposition
751 rate could also be modified due to an absence of soil tillage in the tree rows (Balesdent et al.,
752 1990) or to an increased aggregate stability (Udawatta et al., 2008) in the topsoil.
753
754 **4.2 Representation of SOC spatial heterogeneity in agroforestry systems**
755 The lateral spatial heterogeneity of SOC stocks in the agroforestry plot was well described by
756 the two pools model including priming effect, with higher SOC stocks in the tree rows' topsoil
757 than in the alleys. Inputs from the herbaceous vegetation had an important impact on SOC
758 storage in this agroforestry system. The increased SOC stocks in the tree rows were explained
759 in a big part by an important above-ground carbon input (2.13 t C ha^{-1} yr^{-1}) by the herbaceous
760 vegetation between trees. This result had already been suggested by Cardinael et al., (2015b)
761 and by Cardinael et al., (2017) who showed that even young agroforestry systems could store
762 SOC in the tree rows while trees are still very small. These "grass strips" indirectly introduced
763 by the tree planting in parallel tree rows have a major impact on SOC stocks of agroforestry
764 systems. The model treated the carbon from this herbaceous litter as an input to the upper layer
765 of the mineral soil, in the same way as inputs by roots. Introduction of nitrogen in the model
766 could be further tested in order to take into account a lower carbon use efficiency due to a lack
767 of nutrients for microbial growth in this litter. For all models, SOC stocks were better described
768 in the tree rows than in the alleys. In the alleys, the spatial distribution of organic inputs is more

769 complex and thus more difficult to model. The tree root system is influenced by the soil tillage
770 and by the competition with the crop roots, and thus the highest tree fine root density is not
771 observed in the topsoil but in the 0.3-0.5 m soil layer (Cardinael et al., 2015a). In the model,
772 we were not able to represent this specific tree root pattern with commonly used mathematical
773 functions, and tree root profiles were modeled, by default, using a decreasing exponential.
774 Indeed, piecewise linear functions introduce threshold effects not desirable for transport
775 mechanisms, especially diffusion. This simplification could partly explain the model
776 overestimation of SOC stocks in the 0.0-0.1 m layer of the alleys compared to observed data.
777 This result suggests that it could be useful to couple the CARBOSAF model with a model
778 describing root architecture and root growth (Dunbabin et al., 2013; Dupuy et al., 2010), using
779 for instance voxel automata (Mulia et al., 2010). Moreover, the model described a slight
780 increase of SOC stocks in the middle of the alleys than close to the trees in the alleys. This
781 could be explained by the linear equation used to describe the crop yield as a function of the
782 distance from the trees, leading to an overestimation of the crop yield reduction close to the
783 trees. It could also be explained by the formalism used to model leaf litter distribution in the
784 plot. We considered a homogeneous distribution of leaf inputs in the agroforestry plot, which
785 was the case in the last years, but probably not in the first years of the tree growth where leaves
786 might be more concentrated close to the trees (Thevathasan and Gordon, 1997).
787 The two pools model with priming effect also represented a slight SOC storage in the
788 agroforestry plot below 1.0 m depth, but it was not observed in the field. This could be linked
789 to an overestimation of C input from tree fine root mortality. Indeed, a constant root turnover
790 was considered along the soil profile, but several authors reported a decrease of the root
791 turnover with increasing soil depth (Germon et al., 2016; Hendrick and Pregitzer, 1996; Joslin
792 et al., 2006). However, the sensitivity analysis showed that the model was not sensitive to this
793 parameter (Fig. S4).

794

795 **4.3 Vertical representation of SOC profiles in models**

796 The best model to represent SOC profiles considered the priming effect. This process can act
797 in two different ways on the shape of SOC profiles. It has a direct effect on the SOC
798 mineralization and it therefore modulates the amount of SOC in each soil layer, creating
799 different SOC gradients. This indirectly affects the mechanisms of C transport within the soil
800 profile, as shown by a modification of transport coefficients in the case of priming effect (Table
801 5). Contrary to what was shown by Cardinael *et al.*, (2015c) in long term bare fallows receiving
802 contrasted organic amendments, the addition of another SOC pool could not surpass the
803 inclusion of priming effect in terms of model performance. Together with Wutzler &
804 Reichstein, (2013) and Guenet *et al.*, (2016), this study therefore suggests that implementing
805 priming effect into SOC models would improve model performances especially when
806 modelling deep SOC profiles.
807 We considered here the same transport coefficients for the FOC and HSOC pools, but the
808 quality and the size of OC particles are different, potentially leading to various movements in
809 the soil by water fluxes or fauna activity (Lavelle, 1997). Moreover, we considered identical
810 transport parameters in the agroforestry and in the control plot, but the presence of trees could
811 modify soil structure, soil water fluxes (Anderson et al., 2009), and the fauna activity (Price
812 and Gordon, 1999). However, the model was little sensitive to these parameters (Fig. S4).
813 Further study could investigate the role of different transport coefficients on the description of
814 SOC profiles.
815

816 **4.4 Higher OC inputs or a different quality of OC?**

817 The introduction of trees in an agricultural field not only modifies the amount of litter residues,
818 but also their quality. Tree leaves, tree roots, and the herbaceous vegetation from the tree row

have different C:N ratios, lignin and cellulose contents than the crop residues. Recent studies showed that plant diversity had a positive impact on SOC storage (Lange et al., 2015; Steinbeiss et al., 2008). One of the hypothesis proposed by the authors is that diverse plant communities result in more active, more abundant and more diverse microbial communities, increasing microbial products that can potentially be stabilized. In our model, litter quality is not related to different SOC pools, but is implicitly taken into account in the FOC decomposition rate, which is weighted by the respective contribution from the different types of OC inputs. To test this, we performed a model run considering that all OC inputs in the agroforestry plot were crop inputs (all FOC decomposition rates equaled wheat decomposition rate), but results were not significantly different from the one presented here. We then consider that changes in litter quality in the agroforestry plot did not significantly influence SOC decomposition rates.

4.5 Possible limitation of SOC storage by priming effect

Our modelling results showed that the priming effect could considerably reduce the capacity of soils to store organic carbon. Our study showed that the increase of SOC stocks was not proportional to OC inputs, especially at depth. This result has often been observed in Free Air CO_2 Enrichment (FACE) experiments. In these experiments, productivity is usually increased due to CO_2 fertilization, but several authors also reported an increase in SOC decomposition but not linearly linked to the productivity increase (van Groenigen et al., 2014; Sulman et al., 2014). In this study, the estimation of the priming effect intensity was possible because most OC inputs to the soil were accurately measured. The modelled intensity of priming effect was very strong, offsetting 75 to 90% of potential SOC storage due to OC inputs. In a long-term FACE experiment, Carney *et al.*, (2007) also found that SOC decreased due to priming effect, offsetting 52% of additional carbon accumulated in aboveground and coarse root biomass. The priming effect intensity also relies on nutrient availability (Zhang et al., 2013). In agroforestry

systems, tree roots can intercept leached nitrate below the crop rooting zone (Andrianarisoa et al., 2016), reducing nutrient availability. This beneficial ecosystem service could indirectly increase the priming effect intensity in deep soil layers.

However, this strong intensity could also partially be linked to the formalism used to simulate priming effect. This formalism assumes that there is no mineralisation of the SOC in the absence of fresh OC inputs (no basal respiration). This is a strong hypothesis, but this situation never occurs since the FOC pool is never empty (data not shown). In the alleys and below the maximum rooting depth of crops, there are no direct inputs of FOC, but OC is transported in these deep layers due to transport mechanisms. However, further studies could study the impact of the priming effect formalism on the estimation of its intensity by using explicit microbial biomass for instance (Blagodatsky et al., 2010; Perveen et al., 2014).

Finally, root exudates were not quantified in this study. Several authors showed that they could induce strong priming effects (Bengtson et al., 2012; Keiluweit et al., 2015), but root exudates are also a source of labile carbon, potentially contributing to stable SOC (Cotrufo et al., 2013). These opposing effects of root exudates on SOC should be further investigated, especially concerning the deep roots in agroforestry systems.

5 Conclusions

We proposed the first model that simulates soil organic carbon dynamics in agroforestry accounting for both the whole soil profile and the lateral spatial heterogeneity in agroforestry plots. The two pools model with priming effect described reasonably well the measured SOC stocks after 18 years of agroforestry and SOC distributions with depth. It showed that the increased inputs of fresh biomass to soil in the agroforestry system explained the observed additional SOC storage and suggested priming effect as a process controlling SOC stocks in the presence of trees. This study points out at processes that may be modified by deep rooting trees

and deserve further studies given their potential effects on SOC dynamics, such as additional inputs of C as roots exudates, or altered soil structure leading to modified SOC transport rates.

6 Data availability

The data and the model are freely available upon request and can be obtained by contacting the author (remi.cardinael@cirad.fr).

Information about the Supplement

The Supplement includes the walnut tree fine root biomass (Table S1), the different model performances (Table S2), the potential SOC decomposition rate as a function of soil depth (Fig. S1), the correlation matrix of optimized parameters (Fig. S2), the decoupling of OC inputs and priming effect as a function of soil depth (Fig. S3), and a sensitivity analysis of the model (Fig. S4).

Acknowledgments.

This study was financed by the French Environment and Energy Management Agency (ADEME), following a call for proposals as part of the REACCTIF program (Research on Climate Change Mitigation in Agriculture and Forestry). This work was part of the funded project AGRIPSOL (Agroforestry for Soil Protection, 1260C0042), coordinated by Agroof. Rémi Cardinael was supported both by ADEME and by La Fondation de France. We thank the farmer, Mr Breton, who allowed us to sample in his field. We are very grateful to our colleagues for their work in the field since the tree planting, especially Jean-François Bourdoncle, Myriam Dauzat, Lydie Dufour, Jonathan Mineau, Alain Sellier and Benoit Suard. We thank colleagues and students who helped us for measurements in the field or in the laboratory, especially Daniel Billiou, Cyril Girardin, Patricia Mahafaka, Agnès Martin, Valérie Pouteau, Alexandre Rosa,

and Manon Villeneuve. Finally, we would like to thank Jérôme Balesdent and Pierre Barré for their valuable comments on the modeling part of this work.

References

Ahrens, B., Braakhekke, M. C., Guggenberger, G., Schrumpf, M. and Reichstein, M.: Contribution of sorption, DOC transport and microbial interactions to the ^{14}C age of a soil organic carbon profile: Insights from a calibrated process model, Soil Biol. Biochem., 88, 390–402, 2015.

Albrecht, A. and Kandji, S. T.: Carbon sequestration in tropical agroforestry systems, Agric. Ecosyst. Environ., 99, 15–27, 2003.

Anderson, S. H., Udawatta, R. P., Seobi, T. and Garrett, H. E.: Soil water content and infiltration in agroforestry buffer strips, Agrofor. Syst., 75, 5–16, 2009.

Andrianarisoa, K., Dufour, L., Bienaime, S., Zeller, B. and Dupraz, C.: The introduction of hybrid walnut trees (*Juglans nigra* x *regia* cv. NG23) into cropland reduces soil mineral N content in autumn in southern France, Agrofor. Syst., 90, 193–205, 2016.

Baisden, W. T. and Parfitt, R. L.: Bomb ^{14}C enrichment indicates decadal C pool in deep soil?, Biogeochemistry, 85, 59–68, 2007.

Baisden, W. T., Amundson, R., Brenner, D. L., Cook, A. C., Kendall, C. and Harden, J. W.: A multiisotope C and N modeling analysis of soil organic matter turnover and transport as a function of soil depth in a California annual grassland soil chronosequence, Global Biogeochem. Cycles, 16, 82-1-82–26, 2002.

Balandier, P. and Dupraz, C.: Growth of widely spaced trees. A case study from young agroforestry plantations in France, Agrofor. Syst., 43, 151–167, 1999.

Balesdent, J., Mariotti, A. and Boisgontier, D.: Effect of tillage on soil organic carbon

mineralization estimated from ^{13}C abundance in maize fields, J. Soil Sci., 41, 587–596, 1990.

Bambrick, A. D., Whalen, J. K., Bradley, R. L., Cogliastro, A., Gordon, A. M., Olivier, A. and Thevathasan, N. V: Spatial heterogeneity of soil organic carbon in tree-based intercropping systems in Quebec and Ontario, Canada, Agrofor. Syst., 79, 343–353, 2010.

Bengtson, P., Barker, J. and Grayston, S. J.: Evidence of a strong coupling between root exudation, C and N availability, and stimulated SOM decomposition caused by rhizosphere priming effects, Ecol. Evol., 2(8), 1843–1852, 2012.

Blagodatsky, S., Blagodatskaya, E., Yuyukina, T. and Kuzyakov, Y.: Model of apparent and real priming effects: Linking microbial activity with soil organic matter decomposition, Soil Biol. Biochem., 42(8), 1275–1283, 2010.

Braakhekke, M. C., Beer, C., Hoosbeek, M. R., Reichstein, M., Kruijt, B., Schrumpf, M. and Kabat, P.: SOMPROF: A vertically explicit soil organic matter model, Ecol. Modell., 222, 1712–1730, 2011.

Bruun, S., Christensen, B. T., Thomsen, I. K., Jensen, E. S. and Jensen, L. S.: Modeling vertical movement of organic matter in a soil incubated for 41 years with ^{14}C labeled straw, Soil Biol. Biochem., 39, 368–371, 2007.

Burgess, P. J., Incoll, L. D., Corry, D. T., Beaton, A. and Hart, B. J.: Poplar (*Populus* spp) growth and crop yields in a silvoarable experiment at three lowland sites in England, Agrofor. Syst., 63, 157–169, 2004.

Cardinael, R., Mao, Z., Prieto, I., Stokes, A., Dupraz, C., Kim, J. H. and Jourdan, C.: Competition with winter crops induces deeper rooting of walnut trees in a Mediterranean alley cropping agroforestry system, Plant Soil, 391, 219–235, 2015a.

Cardinael, R., Chevallier, T., Barthès, B. G., Saby, N. P. A., Parent, T., Dupraz, C., Bernoux, M. and Chenu, C.: Impact of alley cropping agroforestry on stocks, forms and spatial

distribution of soil organic carbon - A case study in a Mediterranean context, Geoderma, 259–260, 288–299, 2015b.

Cardinael, R., Eglin, T., Guenet, B., Neill, C., Houot, S. and Chenu, C.: Is priming effect a significant process for long-term SOC dynamics? Analysis of a 52-years old experiment, Biogeochemistry, 123, 203–219, 2015c.

Cardinael, R., Chevallier, T., Cambou, A., Béral, C., Barthès, B. G., Dupraz, C., Durand, C., Kouakoua, E. and Chenu, C.: Increased soil organic carbon stocks under agroforestry: A survey of six different sites in France, Agric. Ecosyst. Environ., 236, 243–255, 2017.

Carney, K. M., Hungate, B. A., Drake, B. G. and Megonigal, J. P.: Altered soil microbial community at elevated CO_2 leads to loss of soil carbon, PNAS, 104, 4990–4995, 2007.

Charbonnier, F., le Maire, G., Dreyer, E., Casanoves, F., Christina, M., Dauzat, J., Eitel, J. U. H., Vaast, P., Vierling, L. A. and Roupsard, O.: Competition for light in heterogeneous canopies: Application of MAESTRA to a coffee (*Coffea arabica* L.) agroforestry system, Agric. For. Meteorol., 181, 152–169, 2013.

Chaudhry, A. K., Khan, G. S., Siddiqui, M. T., Akhtar, M. and Aslam, Z.: Effect of arable crops on the growth of poplar (*Populus deltoides*) tree in agroforestry system, Pakistan J. Agric. Sci., 40, 82–85, 2003.

Chifflot, V., Bertoni, G., Cabanettes, A. and Gavaland, A.: Beneficial effects of intercropping on the growth and nitrogen status of young wild cherry and hybrid walnut trees, Agrofor. Syst., 66, 13–21, 2006.

Clinch, R. L., Thevathasan, N. V., Gordon, A. M., Volk, T. A. and Sidders, D.: Biophysical interactions in a short rotation willow intercropping system in southern Ontario, Canada, Agric. Ecosyst. Environ., 131, 61–69, 2009.

Conant, R. T., Ryan, M. G., Ågren, G. I., Birge, H. E., Davidson, E. A., Eliasson, P. E., Evans,

S. E., Frey, S. D., Giardina, C. P., Hopkins, F. M., Hyvönen, R., Kirschbaum, M. U. F., Lavallee, J. M., Leifeld, J., Parton, W. J., Megan Steinweg, J., Wallenstein, M. D., Martin Wetterstedt, J. Å. and Bradford, M. A.: Temperature and soil organic matter decomposition rates - synthesis of current knowledge and a way forward, Glob. Chang. Biol., 17, 3392–3404, 2011.

Cotrufo, M. F., Wallenstein, M. D., Boot, C. M., Denef, K. and Paul, E.: The Microbial Efficiency-Matrix Stabilization (MEMS) framework integrates plant litter decomposition with soil organic matter stabilization: do labile plant inputs form stable soil organic matter?, Glob. Chang. Biol., 19(4), 988–95, 2013.

Davidson, E. A. and Janssens, I. A.: Temperature sensitivity of soil carbon decomposition and feedbacks to climate change, Nature, 440, 165–173, 2006.

Dimassi, B., Cohan, J.-P., Labreuche, J. and Mary, B.: Changes in soil carbon and nitrogen following tillage conversion in a long-term experiment in Northern France, Agric. Ecosyst. Environ., 169, 12–20, 2013.

Dubbert, M., Mosena, A., Piayda, A., Cuntz, M., Correia, A. C., Pereira, J. S. and Werner, C.: Influence of tree cover on herbaceous layer development and carbon and water fluxes in a Portuguese cork-oak woodland, Acta Oecologica, 59, 35–45, 2014.

Dufour, L., Metay, A., Talbot, G. and Dupraz, C.: Assessing Light Competition for Cereal Production in Temperate Agroforestry Systems using Experimentation and Crop Modelling, J. Agron. Crop Sci., 199, 217–227, 2013.

Dunbabin, V. M., Postma, J. A., Schnepf, A., Pagès, L., Javaux, M., Wu, L., Leitner, D., Chen, Y. L., Rengel, Z. and Diggle, A. J.: Modelling root-soil interactions using three-dimensional models of root growth, architecture and function, Plant Soil, 372, 93–124, 2013.

Dupuy, L., Gregory, P. J. and Bengough, A. G.: Root growth models: Towards a new generation

990 of continuous approaches, J. Exp. Bot., 61, 2131–2143, 2010.

991 Duursma, R. A. and Medlyn, B. E.: MAESPA: a model to study interactions between water
992 limitation, environmental drivers and vegetation function at tree and stand levels, with an
993 example application to [CO_2] × drought interactions, Geosci. Model Dev., 5, 919–940, 2012.

994 Eilers, K. G., Debenport, S., Anderson, S. and Fierer, N.: Digging deeper to find unique
995 microbial communities: The strong effect of depth on the structure of bacterial and archaeal
996 communities in soil, Soil Biol. Biochem., 50, 58–65, 2012.

997 Eissenstat, D. M. and Yanai, R. D.: The Ecology of Root Lifespan, Adv. Ecol. Res., 27, 1–60,
998 1997.

999 Ellert, B. H. and Bettany, J. R.: Calculation of organic matter and nutrients stored in soils under
1000 contrasting management regimes, Can. J. Soil Sci., 75, 529–538, 1995.

1001 Elzein, A. and Balesdent, J.: Mechanistic simulation of vertical distribution of carbon
1002 concentrations and residence times in soils, Soil Sci. Soc. Am. J., 59, 1328–1335, 1995.

1003 Fierer, N., Schimel, J. P. and Holden, P. A.: Variations in microbial community composition
1004 through two soil depth profiles, Soil Biol. Biochem., 35, 167–176, 2003.

1005 Fontaine, S., Barot, S., Barré, P., Bdioui, N., Mary, B. and Rumpel, C.: Stability of organic
1006 carbon in deep soil layers controlled by fresh carbon supply, Nature, 450, 277–281, 2007.

1007 Germon, A., Cardinael, R., Prieto, I., Mao, Z., Kim, J. H., Stokes, A., Dupraz, C., Laclau, J.-P.
1008 and Jourdan, C.: Unexpected phenology and lifespan of shallow and deep fine roots of walnut
1009 trees grown in a silvoarable Mediterranean agroforestry system, Plant Soil, 401, 409–426, 2016.

1010 Graves, A. R., Burgess, P. J., Palma, J. H. N., Herzog, F., Moreno, G., Bertomeu, M., Dupraz,
1011 C., Liagre, F., Keesman, K., van der Werf, W., de Nooy, A. K. and van den Briel, J. P.:
1012 Development and application of bio-economic modelling to compare silvoarable, arable, and
1013 forestry systems in three European countries, Ecol. Eng., 29, 434–449, 2007.

Graves, A. R., Burgess, P. J., Palma, J., Keesman, K. J., van der Werf, W., Dupraz, C., van Keulen, H., Herzog, F. and Mayus, M.: Implementation and calibration of the parameter-sparse Yield-SAFE model to predict production and land equivalent ratio in mixed tree and crop systems under two contrasting production situations in Europe, Ecol. Modell., 221, 1744–1756, 2010.

van Groenigen, K. J., Qi, X., Osenberg, C. W., Luo, Y. and Hungate, B. A.: Faster decomposition under increased atmospheric CO_2 limits soil carbon storage, Science, 344, 508–509, 2014.

Guenet, B., Eglin, T., Vasilyeva, N., Peylin, P., Ciais, P. and Chenu, C.: The relative importance of decomposition and transport mechanisms in accounting for soil organic carbon profiles, Biogeosciences, 10, 2379–2392, 2013.

Guenet, B., Moyano, F. E., Peylin, P., Ciais, P. and Janssens, I. A.: Towards a representation of priming on soil carbon decomposition in the global land biosphere model ORCHIDEE (version 1.9.5.2), Geosci. Model Dev., 9, 841–855, 2016.

Haile, S. G., Nair, V. D. and Nair, P. K. R.: Contribution of trees to carbon storage in soils of silvopastoral systems in Florida, USA, Glob. Chang. Biol., 16, 427–438, 2010.

Hendrick, R. L. and Pregitzer, K. S.: Temporal and depth-related patterns of fine root dynamics in northern hardwood forests, J. Ecol., 84, 167–176, 1996.

Howlett, D. S., Moreno, G., Mosquera Losada, M. R., Nair, P. K. R. and Nair, V. D.: Soil carbon storage as influenced by tree cover in the Dehesa cork oak silvopasture of central-western Spain, J. Environ. Monit., 13, 1897–904, 2011.

Ilstedt, U., Bargués Tobella, A., Bazié, H. R., Bayala, J., Verbeeten, E., Nyberg, G., Sanou, J., Benegas, L., Murdiyarso, D., Laudon, H., Sheil, D. and Malmer, A.: Intermediate tree cover can maximize groundwater recharge in the seasonally dry tropics, Sci. Rep., 6, 21930, 2016.

IUSS Working Group WRB: World Reference Base for Soil Resources 2006, first update 2007. World Soil Resources Reports No. 103. FAO, Rome., 2007.

Jobbagy, E. G. and Jackson, R. B.: The vertical distribution of soil organic carbon and its relation to climate and vegetation, Ecol. Appl., 10, 423–436, 2000.

Joslin, J. D., Gaudinski, J. B., Torn, M. S., Riley, W. J. and Hanson, P. J.: Fine-root turnover patterns and their relationship to root diameter and soil depth in a ^{14}C-labeled hardwood forest, New Phytol., 172, 523–535, 2006.

Kätterer, T., Bolinder, M. A., Andrén, O., Kirchmann, H. and Menichetti, L.: Roots contribute more to refractory soil organic matter than above-ground crop residues, as revealed by a long-term field experiment, Agric. Ecosyst. Environ., 141, 184–192, 2011.

Keiluweit, M., Bougoure, J. J., Nico, P. S., Pett-Ridge, J., Weber, P. K. and Kleber, M.: Mineral protection of soil carbon counteracted by root exudates, Nat. Clim. Chang., 5, 588–595, 2015.

Kim, D.-G., Kirschbaum, M. U. F. and Beedy, T. L.: Carbon sequestration and net emissions of CH_4 and N_2O under agroforestry: Synthesizing available data and suggestions for future studies, Agric. Ecosyst. Environ., 226, 65–78, 2016.

Koarashi, J., Hockaday, W. C., Masiello, C. A. and Trumbore, S. E.: Dynamics of decadally cycling carbon in subsurface soils, J. Geophys. Res., 117, 1–13, 2012.

Koven, C. D., Riley, W. J., Subin, Z. M., Tang, J. Y., Torn, M. S., Collins, W. D., Bonan, G. B., Lawrence, D. M. and Swenson, S. C.: The effect of vertically resolved soil biogeochemistry and alternate soil C and N models on C dynamics of CLM4, Biogeosciences, 10, 7109–7131, 2013.

Lange, M., Eisenhauer, N., Sierra, C. A., Bessler, H., Engels, C., Griffiths, R. I., Mellado-Vázquez, P. G., Malik, A. A., Roy, J., Scheu, S., Steinbeiss, S., Thomson, B. C., Trumbore, S. E. and Gleixner, G.: Plant diversity increases soil microbial activity and soil carbon storage,

1062 Nat. Commun., 6, 6707, 2015.

1063 Lavelle, P.: Faunal activities and soil processes: adaptative strategy that determine ecosystem
1064 function., 1997.

1065 Li, F., Meng, P., Fu, D. and Wang, B.: Light distribution, photosynthetic rate and yield in a
1066 Paulownia-wheat intercropping system in China, Agrofor. Syst., 74, 163–172, 2008.

1067 Lorenz, K. and Lal, R.: Soil organic carbon sequestration in agroforestry systems. A review,
1068 Agron. Sustain. Dev., 34, 443–454, 2014.

1069 Luedeling, E., Smethurst, P. J., Baudron, F., Bayala, J., Huth, N. I., van Noordwijk, M., Ong,
1070 C. K., Mulia, R., Lusiana, B., Muthuri, C. and Sinclair, F. L.: Field-scale modeling of tree-crop
1071 interactions: Challenges and development needs, Agric. Syst., 142, 51–69, 2016.

1072 Manzoni, S., Piñeiro, G., Jackson, R. B., Jobbágy, E. G., Kim, J. H. and Porporato, A.:
1073 Analytical models of soil and litter decomposition: Solutions for mass loss and time-dependent
1074 decay rates, Soil Biol. Biochem., 50, 66–76, 2012.

1075 Mead, R. and Willey, R. W.: The concept of a “land equivalent ratio” and advantages in yields
1076 from intercropping, Exp. Agric., 16, 217–228, 1980.

1077 Moreno, G., Obrador, J. J., Cubera, E. and Dupraz, C.: Fine root distribution in Dehesas of
1078 central-western Spain, Plant Soil, 277, 153–162, 2005.

1079 Moyano, F. E., Vasilyeva, N., Bouckaert, L., Cook, F., Craine, J., Curiel Yuste, J., Don, a.,
1080 Epron, D., Formanek, P., Franzluebbers, A., Ilstedt, U., Kätterer, T., Orchard, V., Reichstein,
1081 M., Rey, A., Ruamps, L., Subke, J. A., Thomsen, I. K. and Chenu, C.: The moisture response
1082 of soil heterotrophic respiration: Interaction with soil properties, Biogeosciences, 9, 1173–
1083 1182, 2012.

1084 Moyano, F. E., Manzoni, S. and Chenu, C.: Responses of soil heterotrophic respiration to
1085 moisture availability: An exploration of processes and models, Soil Biol. Biochem., 59, 72–85,

2013.

Mulia, R. and Dupraz, C.: Unusual fine root distributions of two deciduous tree species in southern France: What consequences for modelling of tree root dynamics?, Plant Soil, 281, 71–85, 2006.

Mulia, R., Dupraz, C. and van Noordwijk, M.: Reconciling root plasticity and architectural ground rules in tree root growth models with voxel automata, Plant Soil, 337, 77–92, 2010.

Nair, P. K.: An introduction to agroforestry, Kluwer Academic Publishers, Dordrecht, The Netherlands., 1993.

Nair, P. K. R.: Classification of agroforestry systems, Agrofor. Syst., 3, 97–128, 1985.

van Noordwijk, M. and Lusiana, B.: WaNuLCAS, a model of water, nutrient and light capture in agroforestry systems, Agrofor. Syst., 43, 217–242, 1999.

Odhiambo, H. O., Ong, C. K., Deans, J. D., Wilson, J., Khan, A. A. H. and Sprent, J. I.: Roots, soil water and crop yield: Tree crop interactions in a semi-arid agroforestry system in Kenya, Plant Soil, 235, 221–233, 2001.

Oelbermann, M. and Voroney, R. P.: And evaluation of the century model to predict soil organic carbon: examples from Costa Rica and Canada, Agrofor. Syst., 82, 37–50, 2011.

Oelbermann, M., Voroney, R. P. and Gordon, A. M.: Carbon sequestration in tropical and temperate agroforestry systems: a review with examples from Costa Rica and southern Canada, Agric. Ecosyst. Environ., 104, 359–377, 2004.

Oelbermann, M., Voroney, R. P., Thevathasan, N. V., Gordon, A. M., Kass, D. C. L. and Schlönvoigt, A. M.: Soil carbon dynamics and residue stabilization in a Costa Rican and southern Canadian alley cropping system, Agrofor. Syst., 68, 27–36, 2006.

Ong, C. K. and Leakey, R. R. B.: Why tree-crop interactions in agroforestry appear at odds with tree-grass interactions in tropical savannahs, Agrofor. Syst., 45, 109–129, 1999.

Parton, W. J., Schimel, D. S., Cole, C. V and Ojima, D. S.: Analysis of factors controlling soil organic matter levels in great plains grasslands, Soil Sci. Soc. Am. J., 51, 1173–1179, 1987.

Peichl, M., Thevathasan, N. V, Gordon, A. M., Huss, J. and Abohassan, R. A.: Carbon sequestration potentials in temperate tree-based intercropping systems, southern Ontario, Canada, Agrofor. Syst., 66, 243–257, 2006.

Perveen, N., Barot, S., Alvarez, G., Klumpp, K., Martin, R., Rapaport, A., Herfurth, D., Louault, F. and Fontaine, S.: Priming effect and microbial diversity in ecosystem functioning and response to global change: A modeling approach using the SYMPHONY model, Glob. Chang. Biol., 20, 1174–1190, 2014.

Price, G. W. and Gordon, A. M.: Spatial and temporal distribution of earthworms in a temperate intercropping system in southern Ontario, Canada, Agrofor. Syst., 44, 141–149, 1999.

Prieto, I., Roumet, C., Cardinael, R., Kim, J., Maeght, J.-L., Mao, Z., Portillo, N., Thammahacksa, C., Dupraz, C., Jourdan, C., Pierret, A., Roupsard, O. and Stokes, A.: Root functional parameters along a land-use gradient: evidence of a community-level economics spectrum, J. Ecol., 103, 361–373, 2015.

Prieto, I., Stokes, A. and Roumet, C.: Root functional parameters predict fine root decomposability at the community level, J. Ecol., 104, 725–733, 2016.

R Development Core Team: R: A language and environment for statistical computing, 2013.

Rasse, D. P., Mulder, J., Moni, C. and Chenu, C.: Carbon turnover kinetics with depth in a French loamy soil, Soil Sci. Soc. Am. J., 70, 2097–2105, 2006.

Salomé, C., Nunan, N., Pouteau, V., Lerch, T. Z. and Chenu, C.: Carbon dynamics in topsoil and in subsoil may be controlled by different regulatory mechanisms, Glob. Chang. Biol., 16, 416–426, 2010.

Santaren, D., Peylin, P., Viovy, N. and Ciais, P.: Optimizing a process-based ecosystem model

with eddy-covariance flux measurements: A pine forest in southern France, Global Biogeochem. Cycles, 21, 1–15, 2007.

Shahzad, T., Chenu, C., Genet, P., Barot, S., Perveen, N., Mougin, C. and Fontaine, S.: Contribution of exudates, arbuscular mycorrhizal fungi and litter depositions to the rhizosphere priming effect induced by grassland species, Soil Biol. Biochem., 80, 146–155, 2015.

Sierra, C. A., Trumbore, S. E., Davidson, E. A., Vicca, S. and Janssens, I.: Sensitivity of decomposition rates of soil organic matter with respect to simultaneous changes in temperature and moisture, J. Adv. Model. Earth Syst., 7, 335–356, 2015.

Soetaert, K., Petzoldt, T. and Woodrow Setzer, R.: Solving Differential Equations in R: Package deSolve, J. Stat. Softw., 33, 1–25, 2010.

Somarriba, E.: Revisiting the past: an essay on agroforestry definition, Agrofor. Syst., 19, 233–240, 1992.

Steinbeiss, S., Beßler, H., Engels, C., Temperton, V. M., Buchmann, N., Roscher, C., Kreutziger, Y., Baade, J., Habekost, M. and Gleixner, G.: Plant diversity positively affects short-term soil carbon storage in experimental grasslands, Glob. Chang. Biol., 14, 2937–2949, 2008.

Sulman, B. N., Phillips, R. P., Oishi, A. C., Shevliakova, E. and Pacala, S. W.: Microbe-driven turnover offsets mineral-mediated storage of soil carbon under elevated CO_2, Nat. Clim. Chang., 4, 1099–1102, 2014.

Taghizadeh-Toosi, A., Christensen, B. T., Hutchings, N. J., Vejlin, J., Kätterer, T., Glendining, M. and Olesen, J. E.: C-TOOL: A simple model for simulating whole-profile carbon storage in temperate agricultural soils, Ecol. Modell., 292, 11–25, 2014.

Talbot, G.: L'intégration spatiale et temporelle du partage des ressources dans un système agroforestier noyers-céréales: une clef pour en comprendre la productivité ?, PhD Dissertation,

Université Montpellier II., 2011.

Tarantola, A.: Inverse problem theory: methods for data fitting and model parameter estimation, edited by Elsevier., 1987.

Tarantola, A.: Inverse Problem Theory and Methods for Model Parameter Estimation, edited by SIAM., 2005.

Thevathasan, N. V. and Gordon, A. M.: Poplar leaf biomass distribution and nitrogen dynamics in a poplar-barley intercropped system in southern Ontario, Canada, Agrofor. Syst., 37, 79–90, 1997.

Udawatta, R. P., Kremer, R. J., Adamson, B. W. and Anderson, S. H.: Variations in soil aggregate stability and enzyme activities in a temperate agroforestry practice, Appl. Soil Ecol., 39, 153–160, 2008.

Virto, I., Barré, P., Burlot, A. and Chenu, C.: Carbon input differences as the main factor explaining the variability in soil organic C storage in no-tilled compared to inversion tilled agrosystems, Biogeochemistry, 108, 17–26, 2012.

van der Werf, W., Keesman, K., Burgess, P., Graves, A., Pilbeam, D., Incoll, L. D., Metselaar, K., Mayus, M., Stappers, R., van Keulen, H., Palma, J. and Dupraz, C.: Yield-SAFE: A parameter-sparse, process-based dynamic model for predicting resource capture, growth, and production in agroforestry systems, Ecol. Eng., 29, 419–433, 2007.

Wutzler, T. and Reichstein, M.: Colimitation of decomposition by substrate and decomposers - a comparison of model formulations, Biogeosciences, 5, 749–759, 2008.

Wutzler, T. and Reichstein, M.: Priming and substrate quality interactions in soil organic matter models, Biogeosciences, 10, 2089–2103, 2013.

Yin, R. and He, Q.: The spatial and temporal effects of paulownia intercropping: The case of northern China, Agrofor. Syst., 37, 91–109, 1997.

Zhang, W., Wang, X. and Wang, S.: Addition of external organic carbon and native soil organic carbon decomposition: a meta-analysis., PLoS One, 8, e54779, 2013.